Development of a model for the simultaneous analysis of wheel and rail wear in railway systems

M. Ignesti, A. Innocenti, L. Marini, E. Meli & A. Rindi

Multibody System Dynamics

ISSN 1384-5640

Multibody Syst Dyn
DOI 10.1007/s11044-013-9360-0

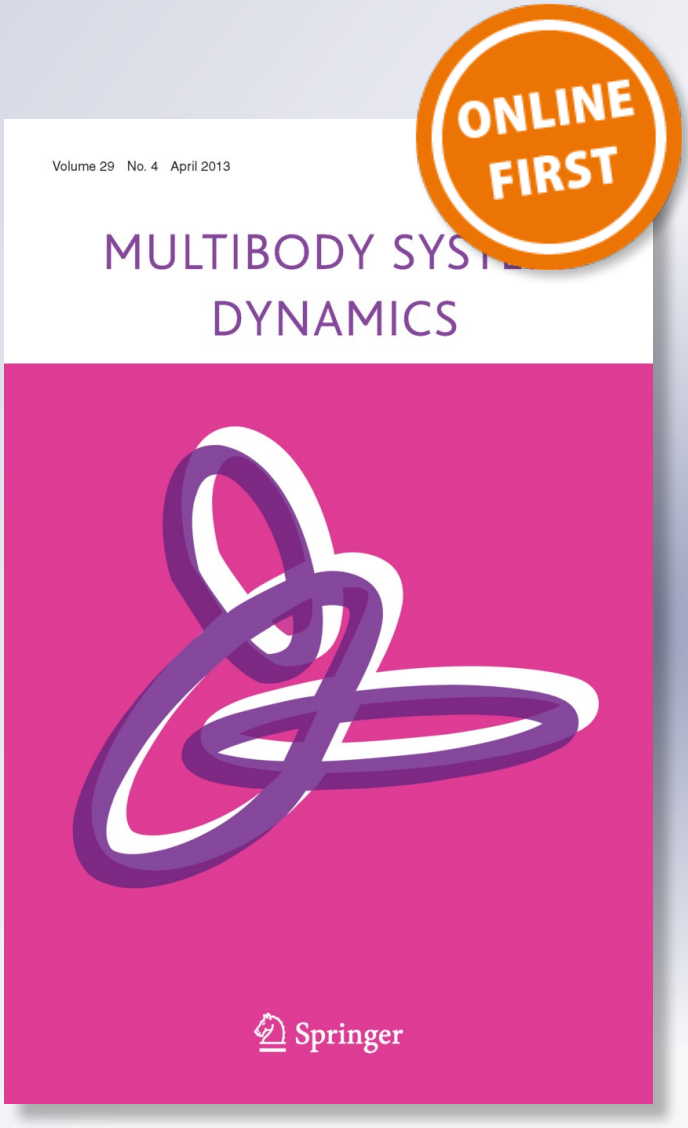

Springer

Your article is protected by copyright and all rights are held exclusively by Springer Science +Business Media Dordrecht. This e-offprint is for personal use only and shall not be self-archived in electronic repositories. If you wish to self-archive your article, please use the accepted manuscript version for posting on your own website. You may further deposit the accepted manuscript version in any repository, provided it is only made publicly available 12 months after official publication or later and provided acknowledgement is given to the original source of publication and a link is inserted to the published article on Springer's website. The link must be accompanied by the following text: "The final publication is available at link.springer.com".

Author's personal copy

Multibody Syst Dyn
DOI 10.1007/s11044-013-9360-0

Development of a model for the simultaneous analysis of wheel and rail wear in railway systems

M. Ignesti · A. Innocenti · L. Marini · E. Meli · A. Rindi

Received: 7 June 2012 / Accepted: 4 March 2013
© Springer Science+Business Media Dordrecht 2013

Abstract The prediction of wheel and rail wear is a fundamental issue in the railway field, both in terms of vehicle stability and in terms of economic costs (planning of maintenance interventions). In particular the need of an accurate wear model arises from the interest of Trenitalia S.p.A. and Rete Ferroviara Italiana in designing new wheel and rail profiles and new bogie architectures optimized from the wear viewpoint with the aim of improving the wear and stability behavior of the standard ORE S1002 wheel profile matched with the UIC60 rail profile canted at 1/20 rad (which represents the wheel–rail combination adopted by the Italian railway line). In this work the authors present a wear model specifically developed for the evaluation of the wheel and rail profile evolution, the layout of which is made up of two mutually interactive but separate units: a vehicle model for the dynamical analysis and a model for the wear evaluation. Subsequently the new model has been compared with the wear evaluation procedure implemented in Simpack, a widely tested and validated multibody software for the analysis of the railway vehicle dynamics; the comparison aims both to evaluate the model performance (in terms of accuracy and efficiency) and to further validate the wear model (just tested, as regards the wheel wear prediction, in previous works related to the critical Aosta–Pre Saint Didier line).

The comparison has been carried out considering a benchmark train composed by a locomotive (E.464) and a passenger vehicle (Vivalto) provided by Trenitalia while the simulations have been performed on a mean Italian railway line (obtained by means of a sta-

M. Ignesti · A. Innocenti · L. Marini · E. Meli (✉) · A. Rindi
Department of Energy Engineering, University of Florence, Via S.Marta n. 3, 50139 Firenze, Italy
e-mail: enrico.meli@unifi.it

M. Ignesti
e-mail: mirko.ignesti@unifi.it

A. Innocenti
e-mail: alice.innocenti@unifi.it

L. Marini
e-mail: lorenzo.marini@unifi.it

A. Rindi
e-mail: andrea.rindi@unifi.it

Published online: 10 April 2013

Author's personal copy

tistical analysis of the data relative to the whole Italian railway network provided by Rete Ferroviaria Italiana (RFI)).

Keywords Multibody modeling · Railway vehicles · Wheel rail wear · Wheel rail contact

1 Introduction

The wear at the wheel–rail interface is a main critical aspect in railway applications; in fact the evolution of the wheel and rail profiles shape that ensues from it has a deep effect both on the dynamics and on the stability of the vehicle causing a running performance variation. From a safety viewpoint the arising of a contact geometry which may compromise the vehicle stability or increase the derailment risk has to be avoid. To this aim the original wheel and rail profiles must be periodically re-established by means of maintenance operations.

Because of these reasons, the development of a mathematical model for the prediction of the wear at the wheel–rail interface represents a very powerful tool to plan the maintenance interventions leading both to an increase of the running safety and a considerable cost saving. A reliable wear model can also be used to optimize the original profiles of wheel and rail and to obtain a more uniform wear. In this way the overall amount of removed material can be reduced in order to increase the mean time between two maintenance intervals and, at the same time, the dynamical performance of the wheel–rail pair can be kept approximately constant between two turnings.

In the literature there are many interesting works dealing with wheel/rail wear modeling based both on global and local approaches to the wear estimation. In the global approach, often used by commercial multibody software to reduce the computational load in spite of the model accuracy [1, 2], the wear is evaluated without taking into account the contact patch. The local approaches [3–5], instead, subdivides the contact patch into adhesion and creep area, leading to more accurate results but increasing the computational time; some works in which the differences between global and local wear approaches are carefully investigated can be found in the literature [17]. However, a substantial lack is present in the literature concerning wear models (both global and even more local) specially developed for complex railway net applications. In this case the computational load needed to carry out the exhaustive simulation of vehicle dynamics and wear evaluation turns out to be absolutely too high for each practical purpose.

Moreover one of main critical aspects in the wear evaluation is the availability of experimental data for the validation of the model, because the wear is a long-term phenomenon which requires several months of monitoring to collect the data; usually the experimental campaigns are carried out only in dry contact condition [6, 7]. If on line experimental measurement cannot be carried out, the problem can be overcome carrying out experimental proofs on a scaled test rig [8], in some case also related to wet contact condition [9].

In this work the authors will present an innovative model to estimate the evolution of the wheel and rail profile due to wear based on the combination of multibody and wear modeling; subsequently an exhaustive comparison with the wear evaluation model implemented in the Simpack commercial multibody software will be performed, both in terms of accuracy and efficiency, to further validate the wear model (in addition to the wheel wear experimental tests carried out in previous works [6, 7]).

The main innovative aspects of the work concern with the application of innovative global contact model in wear problems, the simultaneous treatment of the wheel and rail wear evolution and the statistical track description for the wear process evaluation in extended railway

Author's personal copy

network; this innovative feature will allow complete wear analyses on complex railway track with reasonable computational times for practical purpose unlike the previous wear models.

The general layout of the new model is made up of two mutually interactive parts: the *vehicle model* (multibody model and 3D global contact model) and the *wear model* (local contact model, wear evaluation and profiles update). The multibody model of the vehicle accurately reproduces the vehicle dynamics taking into account all the significant degrees of freedom. The 3D global contact model, developed by the authors in previous works [10, 11], detects the wheel–rail contact points by means of an innovative algorithm based on suitable semi-analytic procedures and then, for each contact point, calculates the contact forces through Hertz's and Kalker's theory [12–14]. As regards the wear estimation, the model is based on a local contact model and on a wear model exploiting an experimental relationship for the calculation of the removed material [8, 15]. The wear model, starting from the outputs of the local contact model (pressures and local creepages), calculates the total amount of removed material due to wear and its distribution along the wheel and rail profiles. The removal of the material is carried out considering the three dimensional structure of the contact bodies and the different time scales characterizing the wear evolution on the wheel and on the rail.

With the only exception of the local contact model, the general architecture of the wear model implemented in Simpack software [16] is similar to that of the new wear model; in this way an accurate comparison between the models has been possible in terms of accuracy and efficiency. In particular the Simpack wear model uses a global approach to the wear estimation that does not consider any local model for the contact patch investigation with a consequent model precision loss [17].

The train set to be investigated in order to evaluate the capability in wear estimation of the two compared wear models is a train composition widely used in Italian railways made up of a locomotive (E.464) and a passenger vehicle (Vivalto) the technical data of which have been provided by Trenitalia S.p.A. [18].

All the simulations are performed on a virtual track, specifically designed to represent a statistical description of the whole Italian railway line [18]. This statistical railway line is a set of N_c curvilinear track characterized, as will be better explained in the following sections, by specific radius R, superelevation h, velocity V and statistical weight p_k (with $1 \leq k \leq N_c$) values. The data necessary to build the virtual track model have been provided by RFI.

The wear model has been experimentally validated in previous works on a benchmark critical scenario (Aln 501 Minuetto traveling on the Aosta–Pre Saint Didier Italian line) [6, 7]. The complete Italian railway network data collection is still in progress but not yet completed because of the task complexity; other tests are scheduled on different particular tracks in order to further investigate advanced wear on the wheel (especially on the wheel tread) and on the rail.

2 General architecture of the model

In this section the layout of the two considered wear models will be described; the innovative model developed in this work will be indicated as UNIFI model, while the benchmark model implemented within the Simpack multibody software will be marked with Simpack model. The main differences between the models in terms of general architecture will be highlighted in the following.

Author's personal copy

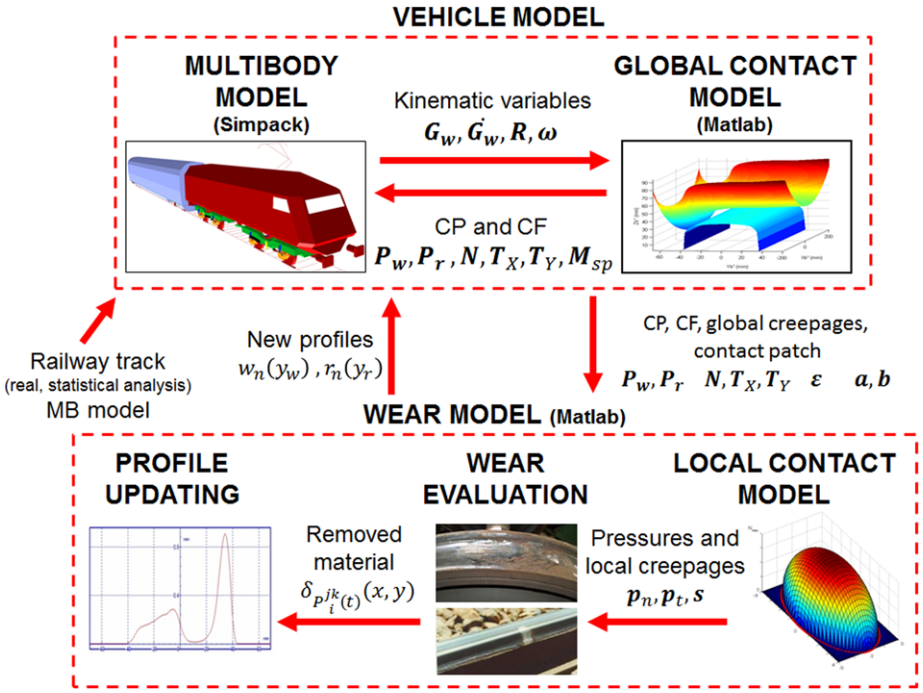

Fig. 1 General architecture of the UNIFI model

2.1 UNIFI wear model layout

The UNIFI model developed in collaboration with Trenitalia and RFI is made up of two main parts: the vehicle model and the wear model (see Fig. 1).

The vehicle model aims to simulate the vehicle dynamics and is composed by the multibody model of the railway vehicle that in this work consists of a locomotive (E.464) and of a passengers vehicle (Vivalto) (a vehicle configuration widely used in the Italian railway network [18]) and by the 3D global contact model; thanks to the numerical efficiency of the innovative contact model, the two models interact directly online during the dynamic simulations at each time integration step creating a loop. In more detail the first one evaluates the kinematic variables (positions, orientations and their derivatives) of the wheelset and consequently of each wheel–rail contact pair while the second one, starting from these quantities, calculates the global contact variables (position of the contact points, geometry of the contact patches by means of the evaluation of its semiaxes, contact forces and global creepages) that are then passed to the multibody model in order to continue the simulation of the vehicle dynamics. The 3D global contact model performs both the detection of the contact points thanks to an innovative algorithm developed by the authors in previous works [10, 11] and the evaluation of the contact forces using Hertz's and Kalker's global theories [12–14]; the algorithm does not introduce any simplifying hypothesis on the geometry and kinematics of the contact problem and can be implemented directly online without using look-up table for the evaluation of the contact variables.

The dynamic simulations have been performed with the Simpack multibody commercial software: the multibody model has been built directly in Simpack environment while the

Author's personal copy

global contact model, implemented in C/C++ environment, has been customized by means of the Simpack *User Routine module* (implemented in FORTRAN environment) capable of handling the interaction between Simpack and routines defined by users.

Besides the multibody model of the considered benchmark vehicle, the other main input of the vehicle model is the railway track; in this research activity the mean Italian railway line has been considered, built by means of a statistical analysis starting from the data relative to the whole Italian railway network (provided by RFI) and consisting of an ensemble of N_c curvilinear tracks, each of length equal to l_{track}, characterized by a radius R, a *superelevation* h, a suitable velocity V and a statistical weight factor p_k [18]. The statistical approach is the same used for the model validation (only related to wheel wear) performed on the Aosta–Pre Saint Didier line [6, 7] and it is obviously necessary because of the length and the complexity of the *considered network* that would make both its multibody modeling and the computational load impractical. The outputs of the vehicle model represent also the inputs of the wear model and are the global contact variables evaluated during all the N_c dynamic simulations.

The wear model has been fully implemented in a Matlab environment and is made up of three distinct phases: the local contact model, the wear evaluation and the profile update. Starting from the global contact variables, the local contact model (based both on Hertz's local theory and on the simplified Kalker's algorithm FASTSIM) evaluates the local contact parameters (the contact pressures and the local creepages) and divides the contact patches into adhesion and slip zone. Then, within the slip area, the distribution of removed material both on the wheel and on the rail surface is calculated by means of an experimental law that correlates the volume of removed material with the frictional dissipated energy at the contact interface. Finally the profiles of wheel and rail are updated by removing the material from the original profiles. The new profiles are the outputs of one discrete step of the whole model loop and have to be passed back to the vehicle model in order to proceed with the wear cycle calculating the vehicle dynamics with the updated profiles.

The evolution of the wheel and rail profiles is therefore a discrete process. In this research the choice of the discrete step is a main issue and, as will be clarified in the following, has to consider the difference between the time scales of the wheel and rail wear evolution rates. For the wheel wear prediction the total mileage km_{tot} traveled by the benchmark vehicle has to be subdivided in discrete steps with a suitable strategy and within each step (corresponding to km_{step} kilometers traveled by the vehicle) the wheel profile will be supposed to be constant. For the rail, instead, the depth of the wear does not depend on the traveled distance but on the total tonnage burden on the track and thus on the number of vehicles moving on the track; particularly the total vehicle number N_{tot} will be subdivided in discrete steps (corresponding to N_{step} vehicles on the track) within which the rail profile is supposed to be constant.

As regards the discretization strategy, the number of discrete steps should be chosen according to a good balance between the model accuracy and the computational load; in fact increasing the step number, the model accuracy increases but, at the same time, the computational load increases too. Furthermore several types of update procedure exist [4, 5]: the constant step and the adaptive step are the main ones. In the first one a constant update step is defined while the second one is based on the definition of a threshold value that imposes the maximum material quantity to be removed at each profiles update; consequently the update step is variable. In this research activity the two methods have been compared and the second one has been chosen due to the following reasons:

1. The adaptive step is more suitable to follow the nonlinear behavior of the wear evolution.

Author's personal copy

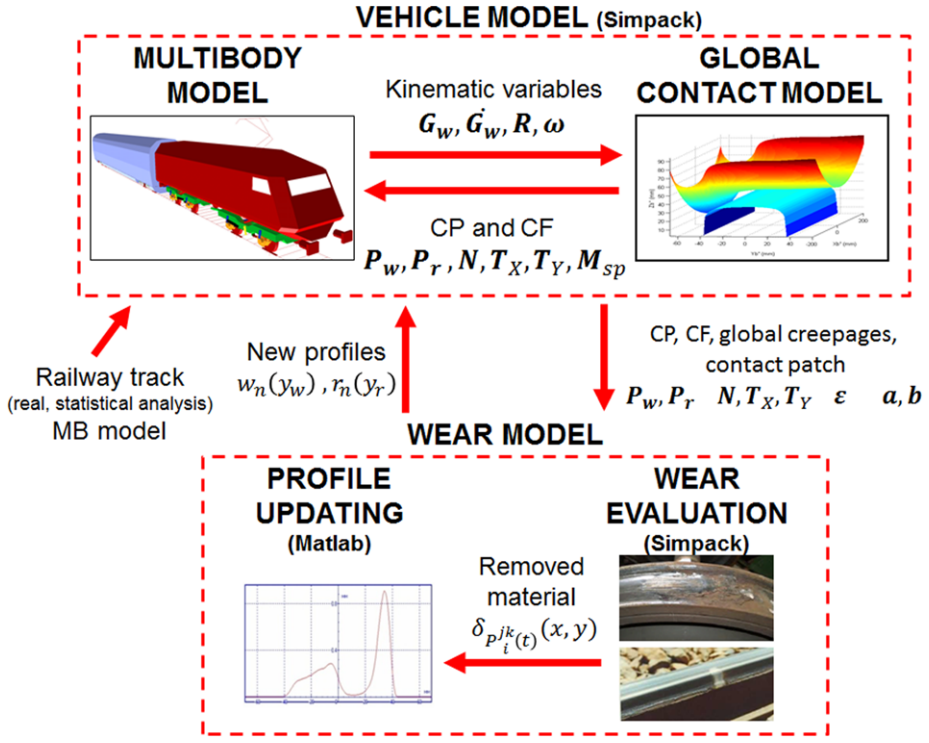

Fig. 2 General architecture of the Simpack model

2. The wear evolution both of wheel and rail in the first phase is characterized by a higher rate because of the initial non-conformal contact between the unworn profiles while in a second phase a slower rate due to the high conformal contact is present. For these reasons an adaptive step follows the wear phenomena better than a constant step.

2.2 Simpack wear model layout

In order to make the comparison between the two wear models more accurate, the Simpack model layout is similar to the UNIFI one, with the exception of the local contact model (see Fig. 2). Therefore the whole model consists of the following parts: the vehicle model fully implemented in Simpack environment (composed by the multibody model and the global contact model) and the global wear model (made up of the wear evaluation directly implemented in Simpack and the profile update implemented in a Matlab environment).

The main difference between the two considered wear models is the approach to the wear problem: the Simpack model uses a global approach to the wear evaluation without taking into account the local contact variables (pressures and creepages) within the contact patch and consequently its subdivision in sliding and adhesion zone but using only the global contact variables. This aspect leads to a reduction of the computational load due to the absence of the contact patch discretization and investigation but it mainly causes a decrease of the whole model precision [17]. Particularly the use of global wear approach involves some handicaps. The improper evaluation of the adhesion and creep zone within the contact patch leads to a likely underestimation or overestimation of the worn material; furthermore

Author's personal copy

the roughness in evaluating the removed material function (due the approximation of the whole contact patch through single contact point) causes both several numerical problems in the wheel and rail profile update procedures and the appearance, in the new profiles, of short wavelengths without physical meaning.

Related to the vehicle model, the benchmark is always the vehicle composition made up of a locomotive (E.464) and a passengers vehicle (Vivalto) and there are no differences with respect to the UNIFI model [18]. On the contrary, concerning the global contact model, the version implemented in the Simpack commercial software has been used. Also this model is capable of calculating the global contact forces and of detecting multiple contact points at the wheel–rail interface; however, for the research of multiple contact points, the wheel and rail surfaces are divided in three different zones within which a single point can be detected, introducing a limitation on the number of contact points and especially on their position. In addition to the simplifying hypothesis on the geometry and kinematics of the contact problem, the Simpack contact model uses look-up table to evaluate the contact parameters with a consequent loss of the model precision.

The profile update strategy has been implemented in a Matlab environment in order both to reproduce the same strategy adopted in the UNIFI model and to adapt it to the wear evaluation model implemented in Simpack (based on a different wear law with respect to the UNIFI model); moreover a new update strategy is necessary because the Simpack model is not designed to simulate a wear loop like that considered by the authors; in particular it is not capable to pass back the new worn profiles to the *vehicle model* to close the loop.

Finally the same considerations explained for the UNIFI model about both the discrete approach of the whole model and the adopted discretization strategy hold also for the Simpack model.

3 The vehicle model

In this section a brief description of the vehicle models (made up of the multibody model and the global contact model) will be given. In particular the global contact models used in the two architectures will be analyzed (the strengths and weaknesses will be emphasized); while, concerning the multibody model, the common benchmark vehicle will be presented.

3.1 The multibody model

A railway vehicle composition widely used on the Italian railway network comprising a E.464 locomotive and a Vivalto passenger transport unit is considered in this work (see Fig. 3); in the following the main characteristics of the multibody models of the two separated units, built in Simpack environment, are described.

3.1.1 E.464 model

The TRAXX 160 DCP, well known with the E.464 commercial name, is a set of light electric locomotives widely used with the passenger vehicles on short and medium distances; its physical and geometrical characteristics can be found in the literature [18, 19]. The E.464 bogies are two motor-axes ones (wheel formula B_0B_0) with two suspension stages for the rigid bodies connections (see Fig. 4). In the multibody modeling the traction elements (motors, gearboxes and auxiliary organs) have been considered part of the frame bogie; the main inertia properties for the vehicle implemented in the multibody model are shown in Table 1.

Author's personal copy

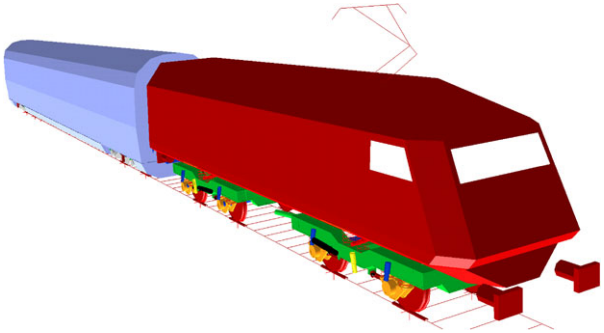

Fig. 3 Global view of the multibody model

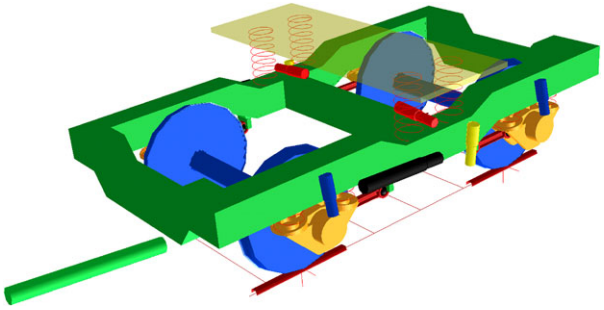

Fig. 4 E.464 model: bogie and suspension stages

Table 1 Inertia properties of the E.464 multibody model

MBS body	Mass (kg)	Roll inertia ($kg \cdot m^2$)	Pitch inertia ($kg \cdot m^2$)	Yaw inertia ($kg \cdot m^2$)
E.464 Coach	43000	61000	524700	524300
E.464 Bogie	10605	1735	6670	8224
E.464 Wheelset	1599	954	220	954

The primary suspension stage (see Fig. 4) is composed by a rigid rod that connects the axlebox with the bogie frame by means of appropriate flexible joints, two coil springs and a damper the arrangement of which is not perfectly vertical to allow the damping of later motions between axlebox and bogie frame. The secondary suspension stage connects the bogie frame to the coach and it comprises four coil springs, six dampers (the verticals ones, the lateral ones and the anti-yaw ones) and a traction rod for the bogie connection to the coach. Both stages of suspensions have been modeled by means of three-dimensional viscoelastic force elements taking into account all the mechanical non-linearities of the dampers. The main linear characteristics of the suspensions are shown in Table 2 while the nonlinear damper characteristics are imposed as a function of the velocity.

3.1.2 Vivalto model

The main feature of the Vivalto coach is the possibility of holding the passengers on two different levels realized in the middle of the carriage. The weight increase resulting from this configuration has led to install three ventilated brake discs for each wheelset, in order to obtain good braking performance. In Table 3 the main inertia properties used for the multibody model are shown [18].

Author's personal copy

Table 2 E.464 model: main linear stiffness properties of the suspensions

MBS element	Longitudinal stiffness (N/m)	Lateral stiffness (N/m)	Vertical stiffness (N/m)	Roll stiffness (N m/rad)	Pitch stiffness (N m/rad)	Yaw stiffness (N m/rad)
Primary suspension coil spring	1730000	1730000	852000	2000000	2000000	2000000
Secondary suspension coil spring	84300	84300	284000	2000000	2000000	2000000

Table 3 Inertia properties of the Vivalto multibody model

MBS body	Mass (kg)	Roll inertia ($kg \cdot m^2$)	Pitch inertia ($kg \cdot m^2$)	Yaw inertia ($kg \cdot m^2$)
Vivalto Coach	50935	128118	2911166	2811166
Vivalto Bogie	2470	1890	2014	3737
Vivalto Wheelset	1410	866	101	866

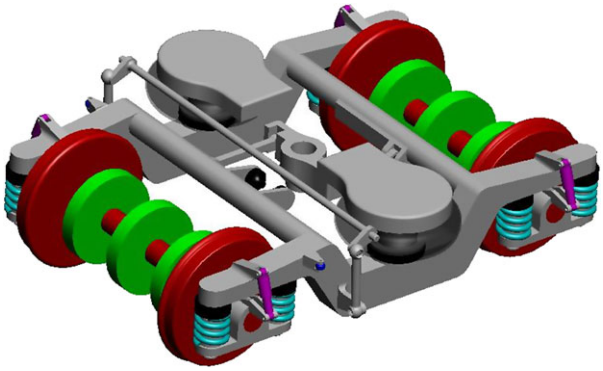

Fig. 5 Vivalto model: bogie and suspension stages

The Vivalto bogies are two trailer bogies with two suspension stages designed by Siemens company, marked SF-400 (see Fig. 5). The primary suspensions are composed by two coil springs and two pivots concentric with the coil springs, forced and welded on the bogie to connect the wheelset; on the pivots suitable rubber springs are fitted. With the particular realized assembly, the coil springs work only in vertical direction while the traction, brake and lateral forces act on the rubber springs. Moreover the primary suspension is equipped with two vertical bumpstops (one for each coil spring) and a damper the arrangement of which is not perfectly vertical for the same reasons treated above.

The secondary suspension is made up of two air springs set up in series at two "emergency springs" which have the purpose to ensure the safety in deflated spring condition; in the modeling a single spring with the characteristic given by the springs mounted in series has been considered. In addition the suspension comprises a common zeta link for the connection between the bogie and the coach, a roll bar necessary because of the rise of the coach center of gravity due to the two passenger levels, two lateral dampers and two lateral bumpstops.

Author's personal copy

Table 4 Vivalto model: main linear stiffness properties of the suspensions

MBS element	Longitudinal stiffness (N/m)	Lateral stiffness (N/m)	Vertical stiffness (N/m)	Longitudinal damping (N s/m)	Lateral damping (N s/m)	Vertical damping (N s/m)
Primary suspension coil spring	–	–	5000000	–	–	2000
Primary suspension rubber spring	5500000	24300000	–	12000	9000	–
Secondary suspension air spring	140000	14000	280000	840	840	25000

Table 5 Vivalto model: roll bar characteristics

MBS element	Roll stiffness (N m/rad)	Roll damping (N m s/rad)
Secondary suspension roll bar	975000	100

The main linear characteristics of the suspensions are shown in Tables 4 and 5, while also in this case the nonlinear damper characteristics are imposed by suitable functions of the velocity.

3.2 The global contact model

Dynamic simulations of railway vehicles need a reliable and efficient method to evaluate the contact points between wheel and rail, because their position has a considerable influence both on the direction and on the magnitude of the contact forces. In this section the two different global contact models used in this research will be described.

3.2.1 UNIFI global contact model

The UNIFI global contact model is divided in two parts: in the first one the contact points are detected by means of an innovative algorithm developed by the Authors in previous works [10, 11], while in the second one the global contact forces acting at the wheel–rail interface are evaluated by means of Hertz's and Kalker's global theories [12–14].

The algorithm for the contact points detection starts from the standard idea that the contact points make stationary the distance between the wheel and rail surfaces (see Fig. 6(a)); in more detail the distance has a point of relative minimum if there is no penetration between the considered surfaces, while it has a relative maximum in the other case. The main features of the innovative adopted algorithm are the following:

– It is a fully 3D model that takes into account all the six relative degrees of freedom (DOF) between wheel and rail.
– It is able to support generic railway tracks and generic wheel and rail profiles.

Author's personal copy

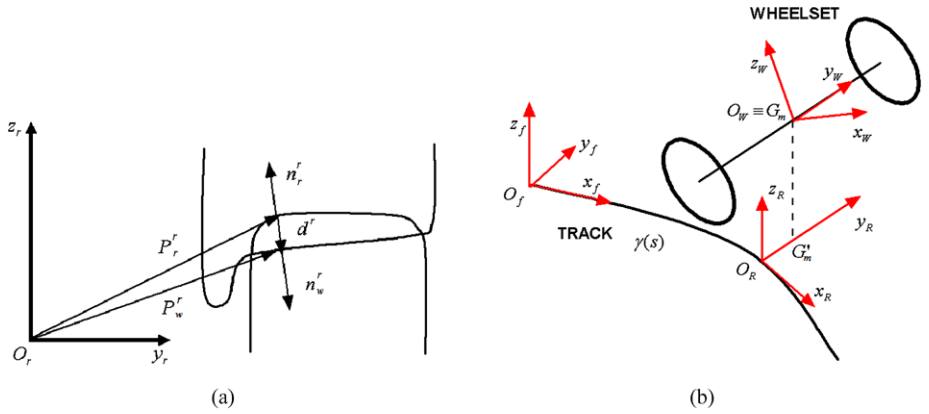

Fig. 6 Distance method

– It ensures a general and accurate treatment of the multiple contact without introducing simplifying assumptions on the problem geometry and kinematics and limits on the number of detected contact points.
– It ensures highly numerical efficiency making possible the online implementation within the commercial multibody software (Simpack—Rail, Adams—Rail) without look-up table; in this way also the numerical performances of the commercial multibody software are improved.

Two specific reference systems have to be introduced in order to simplify the model's equations: the auxiliary reference system and the local reference system. The auxiliary system $O_r x_r y_r z_r$ is defined on the plane of the rails and follows the motion of the wheelset during the dynamic simulations: the x_r axis is tangent to the center line of the track in the origin O_r, the position of which is defined so that the $y_r z_r$ plane contains the center of mass G_w of the wheelset, while the z_r axis is perpendicular to plane of the rails. The local system $O_w x_w y_w z_w$ is rigidly connected to the wheelset (except for the rotation around its axis), its origin O_w coincides with the center of mass G_w of the wheelset, the x_w axis is parallel to the $x_r y_r$ plane and the y_w axis is coincident with the rotation axis of the wheelset (see Fig. 6(b)). In the following, for the sake of simplicity, the variables referred to the local system will be marked with the apex w, while those referred to the auxiliary system with the apex r; the variables belonging to the wheel and to the rail will be indicated with the subscripts w and r, respectively.

Thanks to these reference systems, the definition of the wheel and rail geometrical surfaces is easy. In the local reference system the wheelset can be considered as a simple revolution surface around its axis y_w (see Eq. (2)); the generating function, indicated by $w(y_w)$, is supposed to be known (in this work, the profile ORE S1002 for a single wheel has been chosen (see Fig. 7)). Similarly the track can be locally described in the auxiliary reference system as an extrusion surface along the x_r axis (see Eq. (3)); the generating function, indicated by $r(y_r)$, is known (the profile UIC 60, with laying angle α_p equal to $1/20$ rad, has been chosen for a single rail (see Fig. 7)).

The distance method algorithm (see Fig. 6(a)) is based on a classical formulation of the contact problem in multibody field:

Author's personal copy

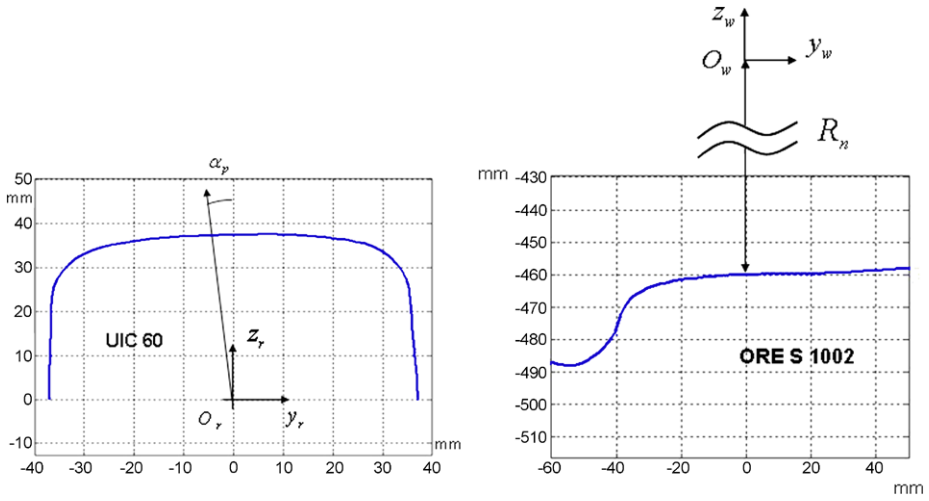

Fig. 7 Wheel and rail profiles

$$\mathbf{n}_r^r\left(\mathbf{P}_r^r\right) \wedge \mathbf{n}_w^r\left(\mathbf{P}_w^r\right) = \mathbf{n}_r^r\left(\mathbf{P}_r^r\right) \wedge R_w^r \mathbf{n}_w^w\left(\mathbf{P}_w^w\right) = \mathbf{0}, \tag{1a}$$

$$\mathbf{n}_r^r\left(\mathbf{P}_r^r\right) \wedge \mathbf{d}^r = \mathbf{0} \tag{1b}$$

where

– $\mathbf{P}_w^w$ and $\mathbf{P}_r^r$ are the positions of the generic points on the wheel surface and on the rail surface expressed in their reference systems:

$$\mathbf{P}_w^w(x_w, y_w) = \left(x_w y_w - \sqrt{w(y_w)^2 - x_w^2}\right)^{\mathrm{T}}, \tag{2}$$

$$\mathbf{P}_r^r(x_r, y_r) = \left(x_r y_r r(y_r)\right)^{\mathrm{T}}; \tag{3}$$

– $\mathbf{n}_w^w$ and $\mathbf{n}_r^r$ are the outgoing normal unit vectors to the wheel and rail surface, respectively, and are defined as follows:

$$\mathbf{n}_w^w\left(\mathbf{P}_w^w\right) = \frac{-\frac{\partial \mathbf{P}_w^w}{\partial x_w} \wedge \frac{\partial \mathbf{P}_w^w}{\partial y_w}}{\| \frac{\partial \mathbf{P}_w^w}{\partial x_w} \wedge \frac{\partial \mathbf{P}_w^w}{\partial y_w} \|}, \qquad \mathbf{n}_r^r\left(\mathbf{P}_r^r\right) = \frac{\frac{\partial \mathbf{P}_r^r}{\partial x_r} \wedge \frac{\partial \mathbf{P}_r^r}{\partial y_r}}{\| \frac{\partial \mathbf{P}_r^r}{\partial x_r} \wedge \frac{\partial \mathbf{P}_r^r}{\partial y_r} \|}; \tag{4}$$

– R_w^r is the rotation matrix that links the local reference system to the auxiliary one;
– $\mathbf{d}^r$ is the distance vector between two generic points on the wheel surface and on the rail surface (both referred to the auxiliary system) and it is equal to

$$\mathbf{d}^r(x_w, y_w, x_r, y_r) = \mathbf{P}_w^r(x_w, y_w) - \mathbf{P}_r^r(x_r, y_r) \tag{5}$$

where $\mathbf{P}_w^r$ is the position of the generic point of the wheel surface expressed in the auxiliary system:

$$\mathbf{P}_w^r(x_w, y_w) = \mathbf{O}_w^r + R_w^r \mathbf{P}_w^w(x_w, y_w). \tag{6}$$

The first condition (Eq. (1a)) of the system (1a), (1b) imposes the parallelism between the normal unit vectors, while the second one (Eq. (1b)) requires the parallelism between the normal unit vector to the rail surface and the distance vector.

Author's personal copy

The system (1a), (1b) consists of six nonlinear equations in the unknowns (x_w, y_w, x_r, y_r) (only four equations are independent and therefore the problem is 4D). However, it is possible to express three of the four variables (in this case (x_w, x_r, y_r)) as a function of y_w, reducing the original 4D problem to a simple 1D scalar equation.

The reduction of the problem dimension using appropriate analytical procedures is the most innovative aspect of the proposed method. Moreover the exact analytical procedures do not introduce simplifying hypotheses for the contact problem resolution, increasing the accuracy and the numerical efficiency of the contact model; therefore it is possible to get much closer to the limit condition of conformal contact (with respect to the other contact models) without particular numerical problems and instabilities. At the same time, in case of conformal contact, finite element (FE) contact models that guarantee the suitable accuracy can be considered to overcome this issue [20, 21]; these FE contact models, specially developed for the railway field, ensure a high numerical efficiency too.

In particular the second component of Eq. (1a) leads to the following equation:

$$r_{13}\sqrt{w(y_w)^2 - x_w^2} = r_{11}x_w - r_{12}w(y_w)w'(y_w) \tag{7}$$

where r_{ij} are the elements of the R_w^r matrix. Calling $A = r_{13}$, $B = w(y_w)$, $C = r_{11}$ and $D = r_{12}w(y_w)w'(y_w)$, the previous equation becomes

$$A\sqrt{B^2 - x_w^2} = Cx_w - D. \tag{8}$$

Hence, removing the radical and solving for x_w:

$$x_{w1,2}(y_w) = \frac{CD \pm \sqrt{C^2D^2 - (A^2 + C^2)(D^2 - A^2B^2)}}{A^2 + C^2}; \tag{9}$$

as can be seen, there are two possible values of x_w for each y_w.

From the first component of Eq. (1a) the following relation for $r'(y_r)$ holds:

$$r'(y_r)_{1,2} = \frac{r_{21}x_{r1,2}(y_w) - r_{22}w(y_w)w'(y_w) - r_{23}\sqrt{w(y_w)^2 - x_{w1,2}(y_w)^2}}{r_{32}w(y_w)w'(y_w) + r_{33}\sqrt{w(y_w)^2 - x_{w1,2}(y_w)^2}}. \tag{10}$$

If $r'(y_r)_{1,2}$ is a decreasing monotonous function (considering separately the sides of the track), Eq. (10) is numerically invertible and a single pair $y_{r\,1,2}(y_w)$ exists for each y_w value; otherwise the numerical inversion is still possible but will produce a further multiplication of the solution number.

By the second component of Eq. (1b) the expression of $x_{r1,2}(y_w)$ can be obtained:

$$x_{r1,2}(y_w) = r_{11}x_{w1,2}(y_w) + r_{12}y_w - r_{13}\sqrt{w(y_w)^2 - x_{w1,2}(y_w)^2}. \tag{11}$$

Finally, replacing the variables $x_{w1,2}(y_w)$, $x_{r1,2}(y_w)$ and $y_{r1,2}(y_w)$ in the first component of Eq. (1b), the following 1D scalar equation can be written:

$$\begin{aligned} F_{1,2}(y_w) = &-r'\left(G_{wz} + r_{32}y_w - r_{33}\sqrt{w^2 - x_{w1,2}{}^2} - r\right) \\ &- \left(G_{wy} + r_{21}x_{w1,2} + r_{22}y_w - r_{23}\sqrt{w^2 - x_{w1,2}{}^2} - y_{r1,2}\right) = 0 \end{aligned} \tag{12}$$

Author's personal copy

where G_{wx}, G_{wy}, G_{wz} are the coordinates of the wheelset center of mass in the auxiliary system. The expression (12) consists of two scalar equations in the variable y_w, which can be easily solved with appropriate numerical algorithms.

The advantages of this approach based on the reduction of the algebraic problem dimension are many and can be summarized as follows:

- The reduction of the algebraic problem dimension from 4D to 1D permits to obtain a high numerical efficiency that makes possible the online implementation of the new method within the multibody vehicle models without look-up table.
- The analytical approach ensures a high degree of accuracy and generality.
- The 1D problem ensures an easier management of the multiple solutions from an algebraic and a numerical point of view.
- In 1D problem also particularly elementary numerical algorithms like the grid method are quite efficient.

Thus, once obtained the generic solution (indicated with the subscript i) y_{wi} of Eq. (12), the complete solution $(x_{wi}, y_{wi}, x_{ri}, y_{ri})$ of the system (1a), (1b) and consequently the contact points $\mathbf{P}^r_{wi} = \mathbf{P}^r_w(x_{wi}, y_{wi})$ and $\mathbf{P}^r_{ri} = \mathbf{P}^r_r(x_{ri}, y_{ri})$ can be found by substitution.

However, since Eqs. (1a), (1b) contain irrational terms, the generic solution $(x_{wi}, y_{wi}, x_{ri}, y_{ri})$ must satisfy the following analytical conditions:

- The solution must be real.
- The solution does not have to generate complex terms (which could be caused by the radicals in the equations).
- The solution must be an effective solution of the system (1a), (1b) (check necessary because of the radical removal by squaring).

Furthermore, from a physical point of view, also the next checks must be evaluated:

- The multiple solutions obtained from the analytical resolution of Eq. (12) must be individuated and erased because they have no physical meaning.
- The following convexity conditions must be satisfied so that the contact is physically possible:

$$k_{1,wi} + k_{1,ri} > 0, \qquad k_{2,wi} + k_{2,ri} > 0 \tag{13}$$

  where $k_{1,wi}, k_{2,wi}$ are the normal curvatures of the wheel surface in longitudinal and lateral direction (referred to the auxiliary system and evaluated in the ith contact point $(x_{wi}, y_{wi}, x_{ri}, y_{ri})$) while $k_{1,ri}, k_{2,ri}$ are the analogous quantities for the rail surface. Because of the problem geometry, the first one of Eq. (13) is always satisfied and thus only the second one must be verified.
- The generic solution of the system (1a), (1b) can be an effective contact point only if the normal penetration $\tilde{p}_n$ between the surfaces of wheel and rail is negative (according to the adopted convention), i.e. there must be effective penetration between the bodies:

$$\tilde{p}_{ni} = \mathbf{d}^r_i \cdot \mathbf{n}^r_r\left(\mathbf{P}^r_{ri}\right) = -\mathbf{d}^r_i \cdot \mathbf{n}^r_w\left(\mathbf{P}^r_{wi}\right) < 0. \tag{14}$$

Then, for each contact point, the normal and tangential contact forces and the global creepages on the contact patch are determined (see Fig. 8).

The normal forces N^r (expressed in the auxiliary system) are calculated by means of Hertz's theory [12]:

$$N^r = \left[-k_h|\tilde{p}_n|^\gamma + k_v|v_n|\frac{\text{sign}(v_n) - 1}{2}\right]\frac{\text{sign}(\tilde{p}_n) - 1}{2} \tag{15}$$

Author's personal copy

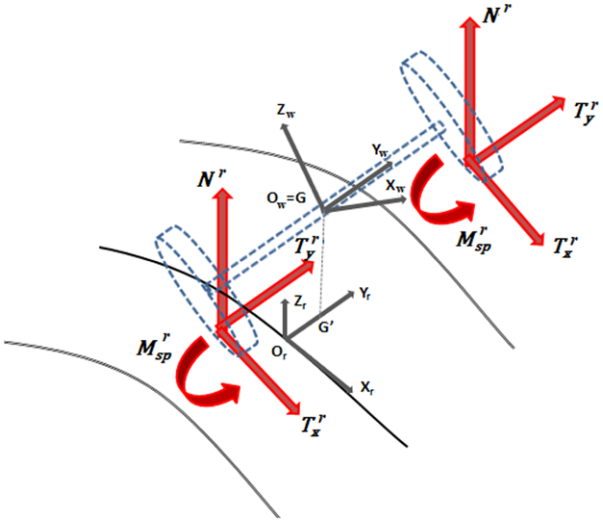

Fig. 8 Global forces acting at wheel and rail interface

where

- $\tilde{p}_n$ is the normal penetration defined by Eq. (14);
- γ is the Hertz exponent equal to 3/2;
- k_v is the contact damping constant ($k_v = 10^5$ N s/m);
- $v_n = \mathbf{V} \cdot n_r^r$ is the normal penetration velocity ($\mathbf{V}$ is the velocity of the contact point rigidly connected to the wheelset);
- k_h is the Hertzian constant, function both of the material properties and of the geometry of the contact bodies (curvatures and semiaxes of the contact patch) [22].

The global creepages $\boldsymbol{\varepsilon}$ (longitudinal ε_x, lateral ε_y and spin creepage ε_{sp}) are calculated as follows:

$$\varepsilon_x = \frac{\mathbf{V} \cdot \mathbf{i}_r}{\|\dot{\mathbf{O}}_w^r\|}, \qquad \varepsilon_y = \frac{\mathbf{V} \cdot \mathbf{t}_r^r(\mathbf{P}_r^r)}{\|\dot{\mathbf{O}}_w^r\|}, \qquad \varepsilon_{\text{sp}} = \frac{\boldsymbol{\omega}_w^r \cdot \mathbf{n}_r^r(\mathbf{P}_r^r)}{\|\dot{\mathbf{O}}_w^r\|} \tag{16}$$

where $\mathbf{V}$ is the velocity of contact point rigidly connected to the wheelset, $\dot{\mathbf{O}}_w^r$ is the wheelset center of mass velocity (taken as the reference velocity for the calculation of the global creepages), $\boldsymbol{\omega}_w^r$ is the angular velocity of the wheelset expressed in the auxiliary system, $\mathbf{i}_r$ is the unit vector in longitudinal direction of the auxiliary system and $\mathbf{t}_r^r$ is the tangential unit vector to the rail profile.

The tangential contact forces $\tilde{T}_x^r$, $\tilde{T}_y^r$ and the spin torque M_{sp}^r (expressed in the auxiliary system) are calculated by means of Kalker's global theory:

$$\tilde{T}_x^r = -f_{11}\varepsilon_x, \qquad \tilde{T}_y^r = -f_{22}\varepsilon_y - f_{23}\varepsilon_{\text{sp}}, \qquad M_{\text{sp}}^r = f_{23}\varepsilon_y - f_{33}\varepsilon_{\text{sp}} \tag{17}$$

where the coefficients f_{ij} are functions both of the materials and of the semiaxes of the contact patch:

$$f_{11} = abGC_{11}, \qquad f_{22} = abGC_{22}, \qquad f_{23} = (ab)^{3/2}GC_{23}, \qquad f_{33} = (ab)^2GC_{33} \tag{18}$$

in which G is the wheel and rail combined shear modulus and C_{ij} are Kalker's coefficients that can be found tabulated in the literature [13]. At this point, it is necessary to introduce a

Author's personal copy

saturation on the tangential contact forces $\tilde{\mathbf{T}}^r = [\,\tilde{T}_x^r \;\; \tilde{T}_y^r\,]^{\mathrm{T}}$ in order to consider the adhesion limit (not taken into account by the linear Kalker's theory):

$$\left\|\mathbf{T}^r\right\| \leq \mu_c N^r \tag{19}$$

where μ_c is the kinetic friction coefficient. Consequently the saturated tangential forces $\mathbf{T}^r$ will have the following expression:

$$\mathbf{T}^r = \varepsilon \tilde{\mathbf{T}}^r \tag{20}$$

in which the saturation coefficient ε can be evaluated as follows [23, 24]:

$$\varepsilon = \begin{cases} \frac{\mu_c N^r}{\tilde{T}^r}\left[\left(\frac{\tilde{T}^r}{\mu_c N^r}\right) - \frac{1}{3}\left(\frac{\tilde{T}^r}{\mu_c N^r}\right)^2 + \frac{1}{27}\left(\frac{\tilde{T}^r}{\mu_c N^r}\right)^3\right] & \text{if } \tilde{T}^r \leq 3\mu_c N^r \\ \frac{\mu_c N^r}{\tilde{T}^r} & \text{if } \tilde{T}^r > 3\mu_c N^r \end{cases} \tag{21}$$

where $\tilde{T}_r = \|\tilde{\mathbf{T}}^r\|$.

3.2.2 Simpack global contact model

The Simpack wear model employs the global contact model implemented in the Simpack multibody software both for the contact points detection and for the global forces calculation [16].

The standard ORE S1002 wheel profile and UIC 60 rail profile with laying angle equal to 1/20 have been introduced in Simpack by means of cubic spline approximation; however, a limitation on the number of profile sampling points (equal to 600 points) is imposed by the software for computational time requirements unlike the UNIFI global contact model, where no limitations are present.

Among all the contact point detection algorithms provided by the software, the more general and suitable version has been chosen in order to compare the two different models. This algorithm ensures multiple contact point detection but, at the same time, introduces a set of simplifying hypotheses:

- A maximum of three contact points for each wheel–rail pair can be detected.
- The wheel profile is divided in three zones called *tread*, *flange* and *flange2* areas: for each of these a single contact point can be found. Moreover the *flange2* corresponds to the back of the flange and thus only two actual contact points for each wheel–rail pair can be detected. The limitation on the contact points position is an important approximation on the kinematics of the contact problem.
- Suitable look-up tables for the calculation of the *tread* contact point location and of the relative tangential forces are used to have reasonable calculation times. The *tread* point is detected considering a quasi-elastic contact. In this case wheel and rail are regarded as qualitatively elastic by means of a special weighting and regularization function (calculated with the look-up table mentioned above): it leads to a virtual contact patch instead of a single contact points and thus no discontinuities can appear with this method.
- The *flange* and *flange2* contacts are calculated online without pre-calculated tables: for these points the wheel–rail contact is considered rigid. With this method, discontinuities in the contact point position and other contact parameters (i.e. tangential forces) can arise when moving the wheelset laterally over the track. The use of different approaches for the contact points detection (in the *tread* and in the *flange* zones) could result in solver and accuracy problems.

Author's personal copy

Concerning to the global normal forces calculation, in the *tread* zone the contact between wheel and rail is ensured by introducing a one-sided spring–damper element (producing a force only when there is penetration between wheel and rail surfaces) which moves along the profiles and the track depending on the contact point position; the normal contact force is calculated from the equivalent penetration by means of the Hertz theory. In the *flange* and *flange2* zones, instead, the wheel–rail contact is ensured by introducing a suitable kinematic constraint while the normal force is the constraint force calculated through the Lagrange multipliers method. The tangential forces evaluation, both for the online calculation in the *flange* and *flange2* zones and for the look-up table calculation in the *tread* zone is based on the linear saturated Kalker theory.

4 The wear model

In this section the wear models will be described in detail: particularly both the two different wear evaluation procedures and the common profile updating strategy will be presented. The update strategy is necessary also for the Simpack model because it is not structured to support a whole wear loop and specifically it is not capable to pass back the new worn profiles to the *vehicle model*. Related to the local contact model, not present in the Simpack model, the Kalker FASTSIM algorithm, widely used in railway applications, has been utilized and its wide and exhaustive description can be found in the literature [13, 25].

4.1 The local contact model

The purpose of the local contact model is the calculation of the local contact variables (normal and tangential contact stresses p_n, $\mathbf{p}_t$ and local creep $\mathbf{s}$, all evaluated within the contact patch) starting from the corresponding global variables (contact points $\mathbf{P}^r_w$, $\mathbf{P}^r_r$, contact forces N^r, T^r_x, T^r_y, global creepage $\boldsymbol{\varepsilon}$ and semiaxes of the contact patch a, b).

For the local analysis a new reference system is defined at the wheel–rail interface on the contact plane (i.e. the common tangent plane between the wheel and rail surfaces): the x and y axes are the longitudinal and the transversal direction of the contact plane, respectively (see Fig. 9). The model is based on Kalker's local theory in the simplified version implemented in the algorithm FASTSIM [13, 25] and consequently on the proportionality hypothesis between the tangential contact pressure $\mathbf{p}_t$ and the elastic displacement $\mathbf{u}$, both evaluated within the contact patch:

$$\mathbf{u}(x, y) = L\mathbf{p}_t(x, y), \quad L = L(\boldsymbol{\varepsilon}, a, b, G, \nu) \tag{22}$$

where the flexibility L is function of the global creepages $\boldsymbol{\varepsilon}$, the semiaxes of the contact patch a, b, the wheel and rail combined shear modulus G and the wheel and rail combined Poisson's ratio ν [13, 25].

The local creepages $\mathbf{s}$ can be calculated by derivation considering both the elastic creepages and the rigid ones:

$$\mathbf{s}(x, y) = \dot{\mathbf{u}}(x, y) + V \begin{pmatrix} \varepsilon_x \\ \varepsilon_y \end{pmatrix} \tag{23}$$

where $V = \|\dot{\mathbf{O}}^r_w\|$ is the longitudinal vehicle speed and ε_x, ε_y are the longitudinal and lateral component of the global creepages $\boldsymbol{\varepsilon}$.

At this point it is necessary to discretize the elliptical contact patch in a grid of points in which the quantities p_n, $\mathbf{p}_t$ and $\mathbf{s}$ will be evaluated. A suitable strategy in which the

Author's personal copy

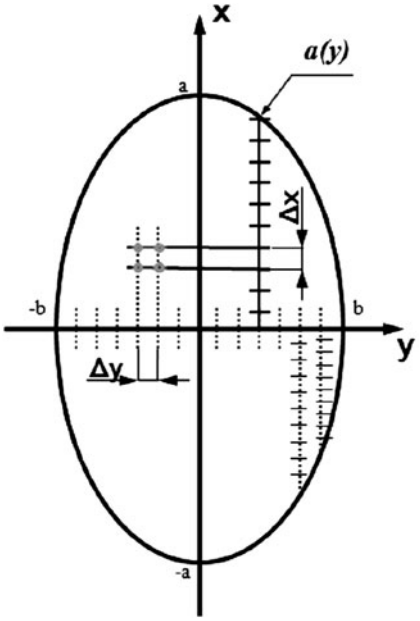

Fig. 9 Contact patch discretization

longitudinal grid resolution is not constant but increases near the lateral edges of the ellipse has been adopted; this procedure provides more accurate results right next to the edges of the ellipse, where a constant resolution grid would generate excessive numerical noise (see Fig. 9) [13].

Once the contact patch is discretized, the FASTSIM algorithm allows the iterative evaluation of both the contact pressures value p_n, $\mathbf{p}_t$ and the local creepage $\mathbf{s}$ in order to divide the contact patch in adhesion and slip zone. Indicating the generic point of the grid with (x_I, y_J), the normal contact pressure is calculated by means of the Hertz local theory:

$$p_n(x_I, y_J) = \frac{3}{2}\frac{N^r}{\pi ab}\sqrt{1 - \frac{x_I^2}{a^2} - \frac{y_J^2}{b^2}} \tag{24}$$

where N^r is the normal contact force while the limit adhesion pressure $\mathbf{p}_A$ is

$$\mathbf{p}_A(x_I, y_J) = \mathbf{p}_t(x_{I-1}, y_J) - \begin{pmatrix} \varepsilon_x \\ \varepsilon_y \end{pmatrix} \frac{\Delta x(y_j)}{L} \tag{25}$$

where $\Delta x(y_J)$ is the longitudinal grid resolution (see Fig. 9). Thus, knowing the variable values in the point (x_{I-1},y_J), it is possible to pass to the point (x_I,y_J) as follows:

$$\text{if } \left\|\mathbf{p}_A(x_I, y_J)\right\| \leq \mu p_n(x_I, y_J)$$

$$\Rightarrow \quad \begin{cases} \mathbf{p}_t(x_I, y_J) = \mathbf{p}_A(x_I, y_J), \\ \mathbf{s}(x_I, y_J) = \mathbf{0}, \end{cases} \tag{26a}$$

$$\text{if } \left\|\mathbf{p}_A(x_I, y_J)\right\| > \mu p_n(x_I, y_J)$$

$$\Rightarrow \quad \begin{cases} \mathbf{p}_t(x_I, y_J) = \mu p_n(x_I, y_J)\mathbf{p}_A(x_I, y_J)/\|\mathbf{p}_A(x_I, y_J)\|, \\ \mathbf{s}(x_I, y_J) = \frac{LV}{\Delta x(y_J)}(\mathbf{p}_t(x_I, y_J) - \mathbf{p}_A(x_I, y_J)) \end{cases} \tag{26b}$$

Author's personal copy

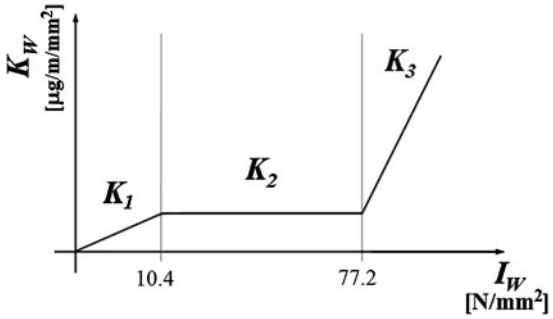

Fig. 10 Trend of the wear rate K_W

where μ is the static friction coefficient; Eqs. (26a) and (26b) hold, respectively, in the adhesion and slip zone.

Iterating the procedure for all the grid discretization points (for $2 \leq I \leq n_x$ and successively for $1 \leq J \leq n_y$) and assuming as boundary conditions $\mathbf{p}_t(x_1, y_J) = \mathbf{0}$, $\mathbf{s}(x_1, y_J) = \mathbf{0}$ for $1 \leq J \leq n_y$ (i.e. stresses and creepages zero out of the contact patch), the desired distributions of $p_n(x_I, y_J)$, $\mathbf{p}_t(x_I, y_J)$ and $\mathbf{s}(x_I, y_J)$ can be determined.

4.2 The UNIFI wear evaluation

The UNIFI model uses an experimental relationship between the volume of removed material and the frictional work [8, 15] to evaluate the distribution of removed material on wheel and rail due to wear (assuming dry contact conditions). The relationship is able to directly evaluate the specific volumes of removed material $\delta_{P_{wi}^{jk}(t)}(x, y)$ and $\delta_{P_{ri}^{jk}(t)}(x, y)$ related to the ith contact points $P_{wi}^{jk}(t)$ and $P_{ri}^{jk}(t)$ on the jth wheel and rail pair during the kth of the N_c dynamic simulations (where $1 \leq i \leq N_{\mathrm{PDC}}$, $1 \leq j \leq N_w$ and $1 \leq k \leq N_C$, indicating with N_{PDC} the maximum number of contact points of each single wheel–rail pair and with N_w the vehicle wheels number).

The calculation of $\delta_{P_i^{jk}(t)}(x, y)$ requires first of all the evaluation of the frictional power developed by the tangential contact stresses; to this purpose the *wear index* I_W (expressed in N/mm^2) is defined as follows:

$$I_W = \frac{\mathbf{p}_t \cdot \mathbf{s}}{V}. \tag{27}$$

This index, by means of appropriate experimental tests, can be correlated with the *wear rate* K_W (expressed in μg/(m $\cdot$ mm^2)) which represents the mass of removed material for unit of distance traveled by the vehicle (expressed in m) and for unit of surface (expressed in mm^2). The wear function between K_W and I_W adopted in this work, is based on twin disk experimental data obtained from the dry coupling between discs made of R8T steel for the wheel and UIC60 900A steel for the rail [8]; the considered couple of materials is widely used in Europe and Italy and also for the vehicles and tracks considered in this research. The experimental relationship is the following (see Fig. 10):

$$K_W(I_W) = \begin{cases} 5.3 \cdot I_W & I_W < 10.4, \\ 55.12 & 10.4 \leq I_W \leq 77.2, \\ 61.9 \cdot I_W - 4723.56 & I_W > 77.2. \end{cases} \tag{28}$$

Once the wear rate $K_W(I_W)$ is known (the same both for the wheel and for the rail), the specific volume of removed material on the wheel and on the rail (for unit of distance

Author's personal copy

traveled by the vehicle and for unit of surface) can be calculated as follows (expressed in $\mathrm{mm}^3/(\mathrm{m}\cdot\mathrm{mm}^2)$):

$$\delta_{P_{wi}^{jk}(t)}(x,y) = K_W(I_W)\frac{1}{\rho}, \tag{29}$$

$$\delta_{P_{ri}^{jk}(t)}(x,y) = K_W(I_W)\frac{1}{\rho} \tag{30}$$

where ρ is the material density (expressed in kg/m^3).

4.3 The Simpack wear evaluation

The Simpack wear model is an add-on module of the Simpack multibody software and allows the calculation of wear effects on the wheel and the rail profiles of a railway vehicle [16]. The wear evaluation is a post-processing calculation after a time domain simulation. The global wear approach leads to the estimation of the removed material starting from the global contact creepages without considering the local ones within the contact patch and therefore this quantity represents an averaged volume to be removed on all the contact patch surface, causing a possible wear overestimation.

This model is based on the wear law proposed by Krause and Poll [1] that correlates the volume of removed material for unit of distance traveled by the vehicle (K^{SIM} expressed in m^3/m) with the specific frictional power I^{SIM} dissipated in the contact patch of area A ($I^{\mathrm{SIM}} = P_g/A$ expressed in W/mm^2: the global power is $P_g = \mathbf{T}^{\mathrm{r}}\cdot\mathbf{s_g}$ where the global creepages $\mathbf{s_g} = V\binom{\varepsilon_x}{\varepsilon_y}$ are expressed in m/s) by means of a proportionality law. It distinguishes between two wear regimes, *mild wear* and *severe wear*, characterized by different removed material rates: the wear coefficients, i.e. the proportionality factors between frictional work and removed material, supposed the same for wheel and rail, are available in the literature [2]:

$$\begin{aligned} &\text{mild wear:} && C_{\mathrm{mild}} = 9.8710\cdot 10^{-14}\ \mathrm{m}^3/\mathrm{J} && I^{\mathrm{SIM}} < 4\ \mathrm{W}/\mathrm{mm}^2, \\ &\text{severe wear:} && C_{\mathrm{severe}} = 9.8710\cdot 10^{-13}\ \mathrm{m}^3/\mathrm{J} = 10\cdot C_{\mathrm{mild}} && I^{\mathrm{SIM}} \geq 4\ \mathrm{W}/\mathrm{mm}^2. \end{aligned} \tag{31}$$

The removed material volume for unit of distance traveled by the vehicle for each wheel and rail is then calculated as follows:

$$K^{\mathrm{SIM}} = \frac{1}{2}\cdot C\cdot\frac{P_g}{V} \tag{32}$$

where C is the proportionality factor of Eq. (31) and V is the velocity of the vehicle.

Finally the average removed material volume (expressed in $\mathrm{m}^3/(\mathrm{m}\cdot\mathrm{mm}^2)$) in the normal direction to the profiles for the ith contact patch of the jth wheel and rail pair during the kth of the N_c dynamical simulations are obtained:

$$\delta^{\mathrm{tot}}_{P_{wi}^{jk}(t)}{}^{\mathrm{SIM}}(y_w) = \begin{cases} 0 & y_w \leq -b_{wi}^{jk}/2, \\ \dfrac{K^{\mathrm{SIM}}}{2\pi w(y_{wi}^{cjk})\cdot b_{wi}^{jk}} & -b_{wi}^{jk}/2 \leq y_w \leq b_{wi}^{jk}/2, \\ 0 & y_w \geq b_{wi}^{jk}/2, \end{cases} \tag{33}$$

Author's personal copy

$$\delta^{\text{tot}}_{P^{jk}_{ri}(t)}{}^{\text{SIM}}(y_r) = \begin{cases} 0 & y_r \le -b^{jk}_{ri}/2, \\ \frac{K^{\text{SIM}}}{l_k \cdot b^{jk}_{ri}} & -b^{jk}_{ri}/2 \le y_w \le b^{jk}_{ri}/2, \\ 0 & y_r \ge b^{jk}_{ri}/2 \end{cases} \tag{34}$$

where $w(y^{cjk}_{wi})$ is the wheel radius evaluated in y^{cjk}_{wi} (the transversal position of the generic wheel contact point), l_k is the length of the kth simulated track ($1 \le k \le N_c$) and b^{jk}_{wi}, b^{jk}_{ri} are the generic contact patch widths. The $1/[2\pi\, w(y^{cjk}_{wi}) \cdot b^{jk}_{wi}]$ and $1/(l_k \cdot b^{jk}_{ri})$ factors average the removed volume for each contact point P^{jk}_i over the whole longitudinal development of the wheel and of the rail.

The global wear evaluation approach, with no local contact model for the investigation of the local variables (pressures and creepages) within the contact patch and therefore no distinction between sliding and adhesion zone in the contact area, leads to the evaluation of the mean wear volumes $\delta^{\text{tot}}_{P^{jk}_{wi}(t)}{}^{\text{SIM}}(y_w)$ and $\delta^{\text{tot}}_{P^{jk}_{ri}(t)}{}^{\text{SIM}}(y_r)$ to be subtracted from the rail and the wheel profiles uniformly along all the contact patch width b. This approximation avoids the contact patch discretization leading to a time calculation saving, but obviously it causes also a decrease of the whole wear model accuracy.

The outputs of the Simpack wear evaluation are thus the distributions of the removed material $\delta^{\text{tot}}_{P^{jk}_{wi}(t)}{}^{\text{SIM}}(y_w)$ and $\delta^{\text{tot}}_{P^{jk}_{ri}(t)}{}^{\text{SIM}}(y_r)$.

4.4 Profile update strategy

The profile update strategy is the set of numerical procedures that allows the calculation of the new profiles of wheel $w_n(y_w)$ and rail $r_n(y_r)$ (the profiles at the next step), starting from the old profiles of wheel $w_o(y_w)$ and rail $r_o(y_r)$ (i.e. the profiles at the current step) and all the distributions of the removed material $\delta_{P^{jk}_{wi}(t)}(x, y)$, $\delta_{P^{jk}_{ri}(t)}(x, y)$ and $\delta^{\text{tot}}_{P^{jk}_{wi}(t)}{}^{\text{SIM}}(y_w)$, $\delta^{\text{tot}}_{P^{jk}_{ri}(t)}{}^{\text{SIM}}(y_r)$ (see Fig. 11). The update strategy is necessary also to remove the numerical noise that affects the previous distributions and that may cause problems to the global contact models due to non-physical alterations of the new profiles. In Fig. 11 the logical correlations among the update steps are shown.

The main procedure steps are described below. For the sake of clarity some preliminary considerations are needed:

- The first procedure step is used only in the UNIFI case.
- The procedure steps 2–4, 6–7 are equal both for UNIFI and Simpack case; for this reason the same variable names will be used for both cases investigated.
- The scaling procedure (fifth procedure step) is different between UNIFI and Simpack cases; therefore the apex SIM will be used to mark the variables.

1. Longitudinal integration: this first integration is related only to the UNIFI model and sums, in the longitudinal direction, all the wear contributes inside the contact patch ($\delta_{P^{jk}_{wi}(t)}(x, y)$ and $\delta_{P^{jk}_{ri}(t)}(x, y)$), averaging this quantity over the whole longitudinal development of the wheel and of the rail (by means of the factors $1/[2\pi\, w(y^{jk}_{wi})]$ and $1/l_k$);

$$\frac{1}{2\pi\, w(y^{cjk}_{wi})} \int_{-a(y)}^{+a(y)} \delta_{P^{jk}_{wi}(t)}(x, y)\, dx = \delta^{\text{tot}}_{P^{jk}_{wi}(t)}(y), \tag{35}$$

$$\frac{1}{l_k} \int_{-a(y)}^{+a(y)} \delta_{P^{jk}_{ri}(t)}(x, y)\, dx = \delta^{\text{tot}}_{P^{jk}_{ri}(t)}(y) \tag{36}$$

Author's personal copy

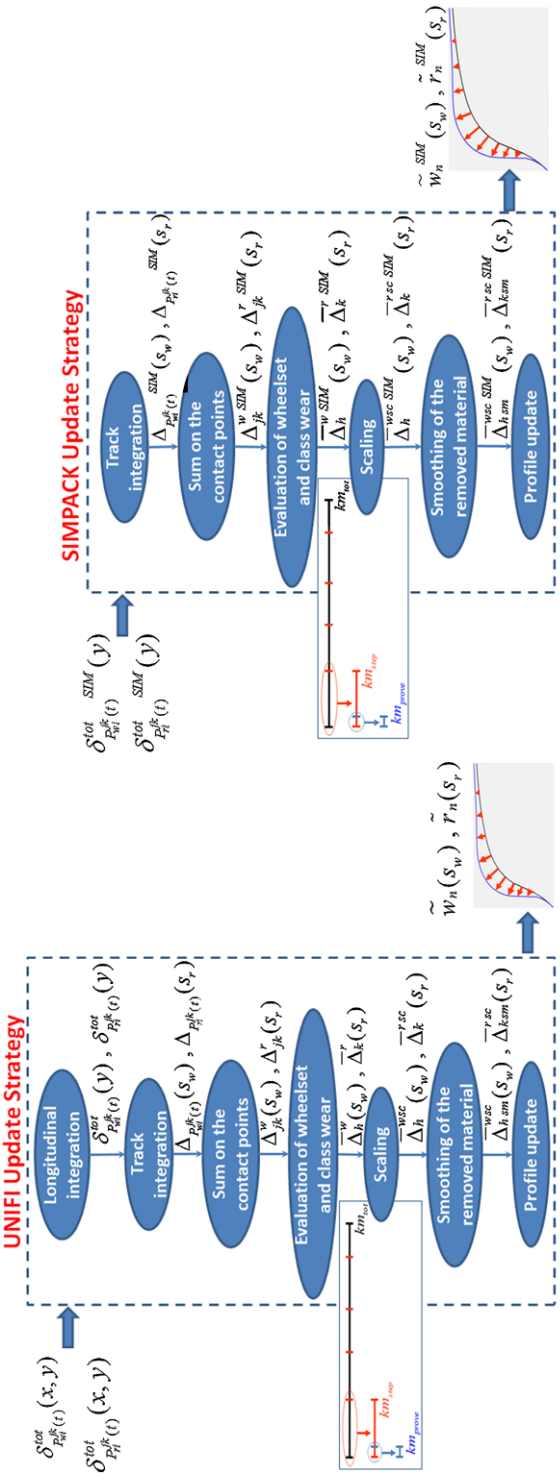

Fig. 11 Profile update strategy

Author's personal copy

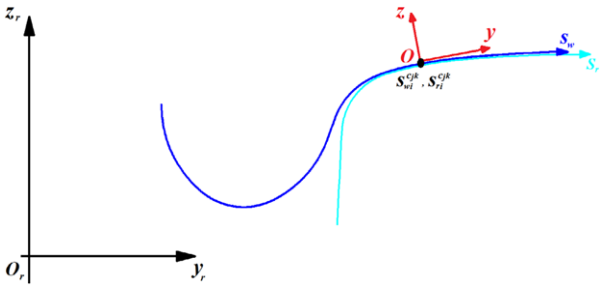

Fig. 12 Normal abscissa for the wheel and rail profile

where $w(y_{wi}^{cjk})$ is the wheel radius evaluated in y_{wi}^{jk} and l_k is the length of the kth simulated track (see also the previous Sect. 4.3). In other words it provides the mean value of removed material expressed in $\mathrm{mm}^3/(\mathrm{m}\cdot\mathrm{mm}^2)$. The difference between the terms $1/l_k$ and $1/[2\pi\, w(y_{wi}^{cjk})]$ (the track length is much greater than the wheel circumference length) is the main cause that leads the wheel to wear much faster than the rail and consequently to a different scale of magnitude of the two investigated phenomena. This reflects the physical phenomenon that the life of the rail is much greater than that of the wheel.

2. Track integration: the track integration sums all the wear contributes coming from the dynamic simulation ($\delta^{\mathrm{tot}}_{P_{ri}^{jk}(t)}(y)$ and $\delta^{\mathrm{tot}}_{P_{ri}^{jk}(t)}(y)$) to obtain the depth of removed material for wheel $\Delta_{P_{wi}^{jk}}(s_w)$ and rail $\Delta_{P_{ri}^{jk}}(s_r)$ expressed in $\mathrm{mm} = \mathrm{mm}^3/\mathrm{mm}^2$;

$$\int_{T_{\mathrm{in}}}^{T_{\mathrm{end}}} \delta^{\mathrm{tot}}_{P_{wi}^{jk}(t)}(y)V(t)\,dt \approx \int_{T_{\mathrm{in}}}^{T_{\mathrm{end}}} \delta^{\mathrm{tot}}_{P_{wi}^{jk}(t)}\left(s_w - s_{wi}^{cjk}(t)\right)V(t)\,dt = \Delta_{P_{wi}^{jk}}(s_w), \tag{37}$$

$$\int_{T_{\mathrm{in}}}^{T_{\mathrm{end}}} \delta^{\mathrm{tot}}_{P_{ri}^{jk}(t)}(y)V(t)\,dt \approx \int_{T_{\mathrm{in}}}^{T_{\mathrm{end}}} \delta^{\mathrm{tot}}_{P_{ri}^{jk}(t)}\left(s_r - s_{ri}^{cjk}(t)\right)V(t)\,dt = \Delta_{P_{ri}^{jk}}(s_r). \tag{38}$$

In order to have a better accuracy in the calculation of the worn profiles, the natural abscissas s_w and s_r of the curves $w(y_w)$ and $r(y_r)$ have been introduced. In particular the following relations locally hold (see Fig. 12):

$$y \approx s_w - s_{wi}^{cjk}(t) \qquad y \approx s_r - s_{ri}^{cjk}(t), \tag{39}$$

$$w(y_w) = w\big(y_w(s_w)\big) = \tilde{w}(s_w) \qquad r(y_r) = r\big(y_r(s_r)\big) = \tilde{r}(s_r) \tag{40}$$

where the natural abscissas of the ith contact points s_{wi}^{cjk} and s_{ri}^{cjk} can be evaluated from their positions P_{wi}^{jk} and P_{ri}^{jk}.

3. Sum on the contact points: this operation enables to calculate the wear depth for each wheel–rail pair ($\Delta_{jk}^{w}(s_w)$ and $\Delta_{jk}^{r}(s_w)$ for wheel and rail respectively) summing the wear contributions of each ith contact point both for wheel $\Delta_{P_{wi}^{jk}}(s_w)$ and rail $\Delta_{P_{ri}^{jk}}(s_w)$:

$$\sum_{i=1}^{N_{\mathrm{PDC}}} \Delta_{P_{wi}^{jk}}(s_w) = \Delta_{jk}^{w}(s_w), \tag{41}$$

$$\sum\nolimits_{i=1}^{N_{\mathrm{PDC}}} \Delta_{P_{ri}^{jk}}(s_r) = \Delta_{jk}^{r}(s_r). \tag{42}$$

Author's personal copy

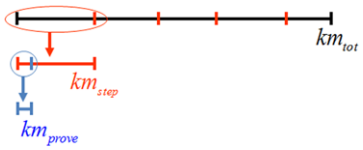

Fig. 13 Discretization of the total mileage

Since the number of contact points on the wheel–rail pair is usually less than N_{PDC} and changes in time during the dynamic simulation, it has been assumed that the wear contribution associated to the fictitious points is zero.

4. Evaluation of wheelset wear and class wear: introducing a new index to indicate the hth vehicle wheelset, the average on the right and left wheels of each wheelset (commonly listed with odd and even index, respectively [26]) is carried out in order to consider the two-way traffic typical for railways vehicle:

$$\Delta^{w}_{hk}(s_w) = 1/2\left(\Delta^{w}_{(2h)k}(s_w) + \Delta^{w}_{(2h-1)k}(s_w)\right)\Big|_{h=1}^{N_w/2} \tag{43}$$

where N_w is the wheels vehicle number. Then the following averages to evaluate for each wheelset the mean wear on all the N_c tracks and for each of the N_c classes the mean rail wear (considering all the wheel–rail pairs) have been performed:

$$\sum_{k=1}^{N_c} p_k \Delta^{w}_{hk}(s_w) = \overline{\Delta}^{w}_{h}(s_w), \tag{44}$$

$$\frac{1}{N_w}\sum\nolimits_{j=1}^{N_w} \Delta^{r}_{jk}(s_r) = \overline{\Delta}^{r}_{k}(s_r). \tag{45}$$

5. Scaling: the aim of the scaling procedure is to amplify the small quantity of material removed during the N_c dynamic simulations and, at the same time, to limit the computational load; assuming the almost linearity of the wear model within a single step of the discrete procedure (valid only if the discretization step length $\mathrm{km_{step}}$ is small enough to consider the profile variation between two consequent steps negligible), it is possible to amplify the removed material by means of a suitable scaling factor.

   The almost linearity of the wear model inside the discrete steps $\mathrm{km_{step}}$ (evaluated with adaptive discretization strategy starting from a fixed constant threshold value on the removed material depth) in which the whole wear evolution $\mathrm{km_{tot}}$ is subdivided, is a working hypothesis coming from the discrete approach of the model. It is based on the idea that the wear rate inside the simulated distance ($\mathrm{km_{prove}}$) remains the same also inside the discrete step $\mathrm{km_{step}}$ (reasonable since the considered vehicle repeats the same railway track both during the simulated distance ($\mathrm{km_{prove}}$) and during the discrete step ($\mathrm{km_{step}}$)).

   In this work an adaptive discrete step (function of the wear rate), obtained imposing the threshold values D^{w}_{step} and D^{r}_{step} on the maximum of the material quantity to be removed on the wheelsets and on the rails at each discrete step, has been chosen to update the wheel and rail profiles (see Eqs. (46)–(51) and Fig. 13): in fact this method well fits in following the behavior of the wear evolution that presents non-linear characteristics outside of the discrete steps.

   The evaluation of the discrete steps, with the consequent scaling of $\overline{\Delta}^{w}_{h}(s_w)$, $\overline{\Delta}^{r}_{k}(s_r)$ and $\Delta^{w\mathrm{SIM}}_{h}(s_w)$, $\Delta^{r\mathrm{SIM}}_{k}(s_r)$, represents the major difference between the update strategy of wheel and rail:

Author's personal copy

(a) The removed material on the wheel due to wear is proportional to the distance traveled by the vehicle; in fact a point of the wheel is frequently in contact with the rail in a number of times proportional to the distance. The following nomenclature can been introduced (see Fig. 13):

- $\mathrm{km}_{\mathrm{tot}}$ is the total mileage traveled by the considered vehicle; its value can be chosen depending on the purpose of the simulations, for example according to the wheelset maintenance European norm [27].
- $\mathrm{km}_{\mathrm{step}}$ is the length of the discrete step corresponding to the threshold value on the wear depth D^w_{step}.
- $\mathrm{km}_{\mathrm{prove}} = l_k$ is the overall mileage traveled by the vehicle during the N_c dynamic simulations; the necessity of acceptable computational times for the multibody simulations leads to adopt small values of the $\mathrm{km}_{\mathrm{prove}}$ length and for this reason the relative removed material has to be scaled with a multiplicative factor.

Finally the material removed on the wheels has to be scaled according to the following laws:

$$\overline{\Delta}_h^{w}(s_w)\frac{D^w_{\mathrm{step}}}{D^w} = \overline{\Delta}_h^{w\mathrm{sc}}(s_w), \qquad \overline{\Delta}_h^{w\mathrm{SIM}}(s_w)\frac{D^w_{\mathrm{step}}}{D^{w\mathrm{SIM}}} = \overline{\Delta}_h^{w\mathrm{scSIM}}(s_w), \tag{46}$$

$$\mathrm{km}_{\mathrm{step}} = \frac{D^w_{\mathrm{step}}}{D^w}\mathrm{km}_{\mathrm{prove}}, \qquad \mathrm{km}_{\mathrm{step}}{}^{\mathrm{SIM}} = \frac{D^w_{\mathrm{step}}}{D^{w\mathrm{SIM}}}\mathrm{km}_{\mathrm{prove}}, \tag{47}$$

where

$$D^w = \max_h \max_{s_w} \overline{\Delta}_h^{w}(s_w), \qquad D^{w\mathrm{SIM}} = \max_h \max_{s_w} \overline{\Delta}_h^{w\mathrm{SIM}}(s_w). \tag{48}$$

The choice of the wear depth threshold must be a good compromise between numerical efficiency and the accuracy required by the wear model. A D^w_{step} too small would provide accurate results but excessive calculation times; the contrary happens with D^w_{step} too big.

(b) The depth of rail wear is not proportional to the distance traveled by the vehicle; in fact the rail tends to wear out only in the zone where it is crossed by the vehicle and, increasing the traveled distance, the depth of removed material remains the same. On the other hand the rail wear is proportional to the total tonnage burden on the rail and thus to the total vehicle number N_{tot} moving on the track. Therefore, if N_{step} is the vehicle number moving in a discrete step, the quantity of rail removed material at each step will be

$$\overline{\Delta}_k^{r}(s_r)\frac{D^r_{\mathrm{step}}}{D^r} = \overline{\Delta}_k^{r\,\mathrm{sc}}(s_r), \qquad \overline{\Delta}_k^{r\,\mathrm{SIM}}(s_r)\frac{D^r_{\mathrm{step}}}{D^{r\,\mathrm{SIM}}} = \overline{\Delta}_k^{r\,\mathrm{scSIM}}(s_r), \tag{49}$$

$$N_{\mathrm{step}} = \frac{D^r_{\mathrm{step}}}{D^r}N_{\mathrm{prove}}, \qquad N_{\mathrm{step}}{}^{\mathrm{SIM}} = \frac{D^r_{\mathrm{step}}}{D^{r\,\mathrm{SIM}}}N_{\mathrm{prove}} \tag{50}$$

where formally $N_{\mathrm{prove}} = 1$ and

$$D^r = \max_k \max_{s_r} \overline{\Delta}_k^{r}(s_r), \qquad D^{r\,\mathrm{SIM}} = \max_k \max_{s_r} \overline{\Delta}_k^{r\,\mathrm{SIM}}(s_r). \tag{51}$$

6. Smoothing of the removed material: the smoothing of the removed material function $\overline{\Delta}_h^{w\,\mathrm{sc}}(s_w)$, $\overline{\Delta}_k^{r\,\mathrm{sc}}(s_w)$ is necessary to remove the numerical noise and short wavelengths

Author's personal copy

without physical meanings that affects this quantity and that would be passed to the new profiles $\tilde{w}_n(s_w)$, $\tilde{r}_n(s_r)$ of wheel and rail causing problems to the global contact models:

$$\Im\left[\overline{\Delta}_h^{w\,\mathrm{sc}}(s_w)\right] = \overline{\Delta}_{h\,\mathrm{sm}}^{w\,\mathrm{sc}}(s_w), \tag{52}$$

$$\Im\left[\overline{\Delta}_k^{r\,\mathrm{sc}}(s_r)\right] = \overline{\Delta}_{k\,\mathrm{sm}}^{r\,\mathrm{sc}}(s_r). \tag{53}$$

To this end, a first-order discrete filter [28] (i.e. a moving average filter with window size equal to 1 %–5 % of the total number of points in which the profiles are discretized) has been used. The main features of this kind of discrete filter are the high numerical efficiency and the mass conservation.

7. Profile update: the last step consists of the update of the old profiles $\tilde{w}_o(s_w) = w_o(y_w)$ and $\tilde{r}_o(s_r) = r_o(y_r)$ to obtain the new profiles $\tilde{w}_n(s_w) = w_n(y_w)$ and $\tilde{r}_n(s_r) = r_n(y_r)$:

$$\begin{aligned}
&\begin{pmatrix} y_w(s_w) \\ \tilde{w}_o(s_w) \end{pmatrix} - \overline{\Delta}_{h\,\mathrm{sm}}^{w\,\mathrm{sc}}(s_w)\mathbf{n}_w^r \xrightarrow{\text{re-parameterization}} \begin{pmatrix} y_w(s_w) \\ \tilde{w}_n(s_w) \end{pmatrix}, \\
&\begin{pmatrix} y_r(s_r) \\ \tilde{r}_o(s_r) \end{pmatrix} - \overline{\Delta}_{k\,\mathrm{sm}}^{r\,\mathrm{sc}}(s_r)\mathbf{n}_r^r \xrightarrow{\text{re-parameterization}} \begin{pmatrix} y_r(s_r) \\ \tilde{r}_n(s_r) \end{pmatrix}.
\end{aligned} \tag{54}$$

Since the removal of material occurs in the normal direction to the profiles ($\mathbf{n}_w^r$ and $\mathbf{n}_r^r$ are the outgoing unit vectors for the wheel and rail profile, respectively), once removed the quantities $\overline{\Delta}_{h\,\mathrm{sm}}^{w\,\mathrm{sc}}(s_w)$, and $\overline{\Delta}_{k\,\mathrm{sm}}^{r\,\mathrm{sc}}(s_r)$, a re-parameterization of the profiles is needed in order to obtain again curves parameterized by means of the curvilinear abscissa.

5 Wear model validation

In this section the comparison between the developed wear model and the Simpack one will be presented. Initially the procedure used to extract the statistical description of the Italian railway network will be introduced, an essential task to make possible and rationalize the approach and the simulation work on a complex railway line: in particular the N_c curvilinear tracks for the dynamic simulations of the considered train composed by the E.464 locomotive and the Vivalto coach will be described. Then the wear control parameters for the wheel and rail will be showed (the flange height FH, the flange thickness FT, the flange steepness QR and the quota QM for the rail). Finally, the simulation strategy used to analyze the wear both on the wheel and on the rail will be described and the results obtained with the UNIFI wear model will be analyzed and compared with the Simpack wear model.

5.1 The statistical approach

When the wear analyses have to be carried out on a set of tracks of considerable length by using at the same time accurate models for the vehicle and the wheel–rail contact, the utilization of "railway line statistical model" may be an indispensable way to overcome a series of problems due to the computational times and the organization of the simulations themselves. The basic idea is to substitute a complex railway network or the too long tracks to be simulated with a set of simpler tracks which can produce an equivalent amount and distribution of wear both on the vehicle wheels and on the rail track.

Author's personal copy

Table 6 Percentage of analyzed data for the Vivalto vehicle

District area	Analyzed distance (km)	Total distance (km)	%
Florence	17934	21588	83.1
Milan	5261	8206	64.1
Bologna	11235	14547	77.2
Genova	1636	1712	95.5
Bari	4667	4668	99.9
Rome	33195	103257	32.1
Total	73929	153978	48.0

In the present work the statistical approach (developed in collaboration with Trenitalia and RFI) has been exploited to draw up the mean line of the considered train [18]. This mean line had to be a significant and equivalent synthesis, in a statistical sense, of the whole set of tracks in Italian railways on which the vehicle composition operates every day. The same strategy has also been used in drawing up a virtual track of the Aosta–Pre Saint Didier line aimed at the wheel wear model validation via comparison with the available experimental data [6, 7].

The methodology is based on the knowledge and the exhaustive analysis of the tracks on which the vehicles operate as well as the relative number of weekly shifts. The shifts are arranged by the district areas of administrative competence of the overall considered railway network of the vehicle composition, which are six: Florence, Milan, Bologna, Genova, Bari and Rome. All data were made available by Trenitalia S.p.A. and Rete Ferroviaria Italiana, as electronic databases, paper plans and paper charts of the single tracks. The extent of the analyzed data for each district area is summarized in Table 6, where actually the distances are the sum of the products between the length of the sections and the relative number of weekly shifts, to take into account the service frequency in each track.

Since the idea is to obtain a set of simple right curved tracks, each of them characterized by curve radius, superelevation height and a traveling speed, as a first step all data for each vehicle have been grouped in radius classes, according to the classification shown in Table 7. The criterion on which the table has been generated is the rigid angle of attack of the wheelsets, that is, the difference in yaw angle between the effective position of the wheelset in the track and the radial position by assuming zero equivalent yaw flexibility in the primary suspensions stage. Consequently, the rigid attack angle is a theoretical borderline case which represents the worst possible condition of guidance because the bogie (or the vehicle, if it is a two-axle vehicle) follows the track maximizing the traveling resistance and the wear in negotiating curves. Conversely, the radial position is usually the condition through which the resistance and the consequent wear are minimized, not to mention the significant benefits in safety against derailment, since even the longitudinal position of the contact patch on the flange of the external wheel is strongly reduced to almost zero.

The rigid attack angle depends only on the bogie wheelbase and the radius of the curve and for this reason it is only an index to classify qualitatively the hypothetical wear severity of curved tracks. The rigid angle attack should not be confused with the effective steady angle of attack of wheelsets in curve (real or in simulation), which depends on other several parameters of the bogie (yaw stiffness, geometric quantities, etc.) as well as the wheel–rail contact condition (friction coefficient); moreover, each wheelset has its own steady angle of attack depending on the position in the bogie (trailing or leading wheelset). The rigid angle represents a superior limit of the steady angle of attack when the yaw stiffness provided by

Author's personal copy

Table 7 Classification intervals

Max rigid angle (mrad)	Min rigid angle (mrad)	Min radius R_m (m)	Max radius R_M (m)	Mean radius R_r (m)
6.0	5.5	208	227	217
5.5	5.0	227	250	238
5.0	4.5	250	278	263
4.5	4.0	278	313	294
4.0	3.5	313	357	333
3.5	3.0	357	417	385
3.0	2.5	417	500	455
2.5	2.0	500	625	556
2.0	1.5	625	833	714
1.5	1.0	833	1250	1000
1.0	0.5	1250	2500	1667
0.5	0.0	2500	10000	5000
0.0	0.0	10000	∞	∞

the primary suspensions (due to a couple of longitudinal stiffness elements which link each axlebox to the bogie frame) tends to infinitive. Bogies designed for high speed trains, having a remarkable stiffness in the primary suspensions, tend to generate angle of attacks similar to the correspondent rigid angle in negotiating sharp curves. On the contrary, the opposite situation, that is, an angle of attack equal to zero, is rarely verified notably for the leading wheelset of a bogie, because it would require a zero yaw stiffness, and this, for reasons due to requirement of stability of the vehicle at high speed, cannot be accepted. Table 7 has been drawn up considering a bogie wheelbase equal to 2.5 m and a step of 0.5 mrad between each class; with simple geometric considerations it has been possible to calculate the minimum and maximum radius values R_m and R_M for each class. The reference radius of each class (R_r) has been simply calculated as the weighted average between the radii included in the class interval $[R_m, R_M]$, using as weights the products between the lengths of the track sections and the number of weekly shifts.

In the statistical approach it is assumed that the wear evolution can be reproduced with a series of simulations on steady curves and straight tracks, neglecting the contribution of the transition lengths (parabolic curves and clothoids [29]) used to connect sections having different superelevation and curve radius. In fact, it would be conceptually difficult to classify and take into consideration these sections; that is the reason why transition lengths have been introduced only in the calculation of the length of the curves, by assigning half length to the curve part and half length to the straight part or to the other adjacent section in case of consecutive curves. For all the missing transition lengths, the information of which were not available, a reasonable length has been introduced on the basis of the maximum allowable roll speed $\Omega \leq 0.038\ \mathrm{rad\,s^{-1}}$ and the maximum allowable derivative of the non-compensated acceleration (Eq. (55)), equal to $\Psi \leq 0.35\ \mathrm{m\,s^{-3}}$ (see below) for the rank to which the vehicle belongs [29]. First of all, the instantaneous non-compensated acceleration for a railway vehicle running in a curve (Fig. 14) is defined as

$$a_{\mathrm{nc}} = \frac{V^2}{R} - g\frac{h}{s_t}, \tag{55}$$

Author's personal copy

Fig. 14 Accelerations in curve

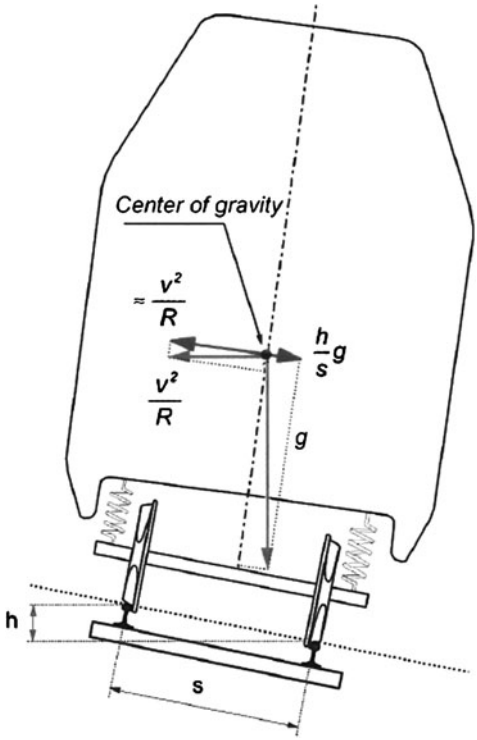

in which V is the constant vehicle speed, R is the curve radius, h is the superelevation height, g the gravitational acceleration and s_t the nominal distance (1500 mm) between the two contact points on the wheelset when it is centered on the track. The approximated expressions of Ω and Ψ are instead the following:

$$\Omega \cong \frac{\Delta h \cdot V}{s_t l}, \tag{56a}$$

$$\Psi \cong \frac{V \cdot \Delta a_{\mathrm{nc}}}{l}, \tag{56b}$$

where Δh and s_t are expressed in mm, V is the constant vehicle speed in the transition sections (in m/s), Δa_{nc} (m/s^2) is the variation in non-compensated acceleration and l (in m) the length of the transition section. The two above mentioned criteria can be satisfied at the same time by choosing an opportune value for the superelevation gradients dh/ds with respect to the curvilinear abscissa s of the track in the range 1–1.5 ‰, considering that $dh/ds \cdot l \cong \Delta h$.

The further division of each radius class in superelevation classes has been arranged as listed below, by grouping the classes of superelevation in five groups and choosing a few height value in each of them, since in reality the superelevation heights are usually rounded to the nearest centimeter (see Table 8).

For the purpose of the dynamic simulations, each superelevation class is represented by the value (h_r) to which corresponds the highest sum of products between section lengths and number of weekly shifts.

Author's personal copy

Table 8 Superelevation classes

Superelevation range	Superelevation value			
0				
10–40	10	20	30	40
50–80	50	60	70	80
90–120	90	100	110	120
130–160	130	140	150	160

	Superelevation (mm)																
	0	10-40				50-80					90-120				130-160			
Mean radius (m)	0	10	20	30	40	50	60	70	80	90	100	110	120	130	140	150	160
217	45	45	50	50	50	55	55	55	60	60	60	65	65	65	65	70	70
238	45	50	50	55	55	55	60	60	60	65	65	65	65	70	70	70	75
263	50	50	55	55	60	60	60	65	65	65	70	70	70	70	70	75	75
294	55	55	55	60	60	65	65	65	70	70	70	70	70	75	75	80	80
333	55	60	60	65	65	65	70	70	70	70	70	70	75	80	80	85	85
385	60	65	65	70	70	70	70	70	70	70	75	75	80	85	85	90	95
455	65	70	70	70	70	70	70	70	70	75	80	85	90	90	95	100	100
556	70	70	70	70	70	70	70	75	80	85	90	95	95	100	105	110	115
714	70	70	70	70	70	70	80	85	90	95	100	105	110	115	120	125	130
1000	70	70	70	70	75	85	90	100	105	115	120	125	130	135	140	145	150
1667	70	70	70	85	95	110	120	130	140	145	155	160	160	160			
5000	70	85	120	145	160												

Fig. 15 B-rank speed table: values of speed V_r as function of radius curve R_m and superelevation h_r

As regard the speed V_r to be assigned to each track in the mean line, the choice has been made according to the table in Fig. 15, which summarizes the speeds in km/h to be observed by B-rank vehicles. In fact, there are four different rank classes in Italy (P, C, B, and A, in descending order of quality) which generally have to observe different speed limits in the same track.

For each combination of curve radius and superelevation, the speed is chosen sufficiently high, according to a certain criterion: as depicted in the speed table, three criteria (corresponding to different sectors of the table) are taken into account. In order to explain the procedure, first of all from the Eq. (55) the expression of the balancing speed $\hat{V}$ for which the non-compensated acceleration vanishes can be derived, being the centrifugal force exactly balanced by the component of the gravitational force along the tangent plane to the track:

$$a_{\mathrm{nc}} = 0 \quad \Rightarrow \quad \hat{V} = \sqrt{\frac{Rgh}{s_t}}. \tag{57}$$

After changing the units to have the track distance s_t in mm, the speed in km/h and the superelevation in mm, Eq. (57) becomes

$$h = 11.8\frac{\hat{V}^2}{R}; \tag{58}$$

also, by introducing the maximum allowable speed in the track V_r and a coefficient c, such that $\hat{V} = cV_r$, taking into account Eqs. (55), (57), and (58) the following system can be

Author's personal copy

written:

$$\begin{cases} h = \frac{11.8}{R}(cV_r)^2, \\ a_{\text{nc}} = \frac{V_r^2}{12.96 \cdot R}(1 - c^2), \end{cases} \tag{59}$$

in which h and R are known while the unknowns are V_r, c and a_{nc}.

By expressing s_t and h in mm, the radius curve R in m, the speeds V_r (in km/h) are chosen as clarified below:

Dark sky blue sector The speeds in this sector are chosen by setting $c = 0.8$ in the system (59) regardless of the resulting value of a_{nc}, so that the theoretical expression $\tilde{V}_r$ of the speed V_r becomes

$$\tilde{V}_r = 1.06\sqrt{\frac{Rh}{7.55}}\ \text{(km/h)}, \tag{60}$$

where the radius curve is in m and the height of superelevation is in mm; the height of superelevation is hence proportional to the centrifugal acceleration. The factor 1.06 means that the speed can be further increased by 6 % with respect to the value included in the radical, because the vehicle belongs to the B-rank class. The effective speed for each radius-superelevation combination is then chosen as

$$V_r = \min(\tilde{V}_r, 160)\ \text{(km/h)}; \tag{61}$$

Yellow sector

$$\tilde{V}_r = 3.6\sqrt{R\left(\frac{gh}{s_t} + 0.8\right)}\ \text{(km/h)}; \tag{62}$$

in the yellow part the $\tilde{V}_r$ speed of each subtrack is chosen according to Eq. (62) after setting a non-compensated acceleration equal 0.8 m/s^2 in the system (59), regardless of the consequent value of c. The effective value has to be chosen as

$$V_r = \min(\tilde{V}_r, 70)\ \text{(km/h)}. \tag{63}$$

Light sky blue sector

$$V_r = 70\ \text{km/h}; \tag{64}$$

this sector represents a connection zone between the two zones mentioned above. The speed is set equal to 70 km/h everywhere.

Regardless of the sector, the final speeds are finally rounded down to the nearest multiple of 5 km/h.

Finally the application of the criteria explained in this section has provided the mean line reported in Table 9, made up of 33 classes (the non-existent radius—superelevation classes are not listed for brevity). For each subtrack the mean radius R_r, the speed V_r, the superelevation h_r as well as the statistical weight p_k have been specified. This latter ($0 \leq p_k \leq 1$) is a weighting factor for the wear evaluation taking into account the frequency of each subtrack within the whole statistical analysis of the Italian railway network.

Author's personal copy

Table 9 Virtual track

R_m (m)	R_M (m)	R_r (m)	h_{range} (mm)	h_r (mm)	V_r (km/h)	p_k %
278	313	**294**	90–120	100	70	0.04
			130–160	140	75	0.03
313	357	**333**	90–120	120	75	0.74
			130–160	160	85	0.74
357	417	**385**	50–80	60	70	0.82
			90–120	90	70	0.07
			130–160	160	85	0.19
417	500	**455**	50–80	50	70	0.03
			90–120	120	90	0.20
			130–160	150	100	1.76
500	625	**556**	10–40	30	70	0.02
			50–80	60	70	0.15
			90–120	120	95	0.36
			130–160	140	105	1.29
625	833	**714**	10–40	20	70	0.03
			50–80	80	90	0.25
			90–120	90	95	1.14
			130–160	160	130	1.93
833	1250	**1000**	10–40	40	70	0.07
			50–80	80	105	1.87
			90–120	120	130	1.80
			130–160	160	150	2.05
1250	2500	**1667**	0	0	70	0.09
			10–40	40	95	0.56
			50–80	80	140	2.27
			90–120	110	160	1.78
			130–160	160	160	0.73
2500	10000	**5000**	0	0	70	0.51
			10–40	30	145	3.96
			50–80	50	160	2.12
			90–120	90	160	0.003
∞					160	74.4

5.2 Wear control parameters

The reference quota FH, FT, and QR are introduced in order to estimate the wheel profile evolution due to the wear without necessarily knowing a complete detection of the profile shape (see Fig. 16). According to these quota it will be possible both to establish when the worn wheel profile will have to be re-profiled and to detect if the wear compromises the dynamical stability of the vehicle (see the current European Standard [27]).

The procedure to define the reference quota and the nomenclature adopted are the following:

Author's personal copy

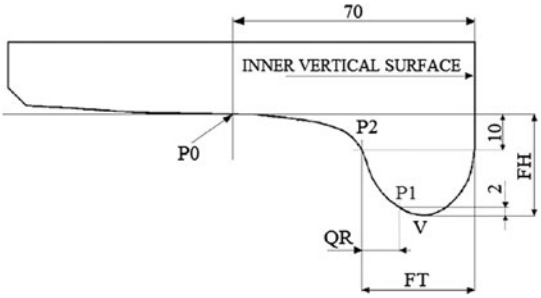

		$d \leq 630$	$630 < d \leq 760$	$760 < d$
fH	min	31.5	29.5	27.5
	max		36	

		$d \leq 760$	$760 < d \leq 840$	$840 < d$
fT	min	27.5	25	22
	max		33	

qR	min	6.5

Fig. 16 Reference dimensions of the wheel profile (*left*) and limit values in mm (*right*) for a wheel having an actual rolling diameter equal to d

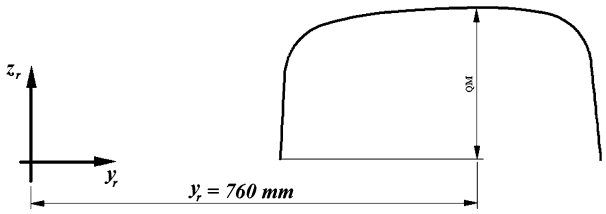

Fig. 17 Definition of rail wear control parameter

1. The point $P0$ is defined on the profile, at 70 mm from the internal vertical face of the wheel.
2. The point $P1$ is 2 mm above the flange vertex on the profile.
3. The point $P2$ is determined on the profile, 10 mm under the point $P0$.
4. The flange thickness FT is the horizontal distance between the internal vertical face and the point $P2$; the flange steepness QR is the horizontal distance between the points $P1$ and $P2$, while the flange height FH is the vertical distance between $P0$ and the flange vertex (all the distances are considered positive).

Because of the way in which they are defined, the quota are positive and do not depend on the wheel rolling radius. In regard to their physical meaning, both the flange thickness FT and the flange height FH describe the size of the flange, while the flange height is also a measure of the wear on the wheel tread. The QR dimension gives information related to the conicity of the flange.

An additional control parameter is then introduced to evaluate the evolution of rail wear. Particularly the QM quota are defined as the rail head height in the point $y_r = 760$ mm with respect to the center line of the track: this y_r value depends on the railway gauge (equal to 1435 mm in the Italian railway line) and on the laying angle α_p of the track (equal to $1/20$ rad). Physically the QM quota give information on the rail head wear (see Fig. 17).

5.3 Simulation strategy

In this section the simulation campaign performed to study the wear on wheel and rail is described. As explained in Sect. 4.4, the two phenomena evolve according to different time scales (several orders of magnitude) and a fully simulation of such events would require a too heavy computational effort. For this reason the following specific algorithm has been adopted for updating the profiles:

Author's personal copy

1. A suitable number of discrete steps both for the wheel and for the rail steps have been chosen, $n_{sw} = 15$ and $n_{sr} = 5$, so to have a good compromise between calculation times and result accuracy:
   (a) Consequently the wheel wear threshold D^w_{step} (see Sect. 4.4) has been chosen equal to 0.4 mm.
   (b) The value of the rail wear threshold D^r_{step} (see Sect. 4.4) has been set equal to 0.8 mm to obtain an appreciable rail wear during the simulations.
2. The wear evolutions on wheel and rail have been decoupled because of the different scales of magnitude:
   (a) While the wheel wear evolves, the rail is supposed to be constant: in fact, in the considered time scale, the rail wear variation is negligible.
   (b) Because of the time scale of the rail wear, each discrete rail profile comes in contact, with the same frequency, with each possible wheel profile. For this reason, for each rail profile, the whole wheel wear evolution (from the original profile to the final profile) has been simulated.

Based on the two previous hypotheses, the simulations have been carried out according to the following strategy:

$$
\begin{aligned}
&\textbf{Wheel profile evolution at first rail step: } w_{h_i}^{0}\\
&p_{1,1}\left\{\left(w_{h_0}^{0} \quad r_{k0}\right) \rightarrow \left(w_{h_1}^{0} \quad r_{k0}\right) \rightarrow \cdots \rightarrow \left(w_{h_{n_{sw}-1}}^{0} \quad r_{k0}\right) \rightarrow w_{h_{n_{sw}}}^{0}\right.\\
&\textbf{Average on the rails } r_{k_1}^{(i+1)} \textbf{ for the calculation of the second rail step: } r_{k1}\\
&p_{1,2}\left\{\begin{pmatrix} w_{h_0}^{0} & r_{k0} \\ w_{h_1}^{0} & r_{k0} \\ \vdots & \vdots \\ w_{h_{n_{sw}-1}}^{0} & r_{k0} \end{pmatrix} \rightarrow \begin{pmatrix} r_{k_1}^{(1)} \\ r_{k_1}^{(2)} \\ \vdots \\ r_{k_1}^{(n_{sw})} \end{pmatrix} \rightarrow r_{k1}\right.\\
&\vdots\\
&\textbf{Wheel profile evolution at } n_{sr}-1 \textbf{ rail step: } w_{h_i}^{n_{sr}-1}\\
&p_{n_{sr},1}\left\{\begin{array}{l}\left(w_{h_0}^{n_{sr}-1} \quad r_{kn_{sr}-1}\right) \rightarrow \left(w_{h_1}^{n_{sr}-1} \quad r_{kn_{sr}-1}\right)\\ \quad \rightarrow \cdots \rightarrow \left(w_{h_{n_{sw}-1}}^{n_{sr}-1} \quad r_{kn_{sr}-1}\right) \rightarrow w_{h_{n_{sw}}}^{n_{sr}-1}\end{array}\right.\\
&\textbf{Average on the rails } r_{kn_{sr}}^{(i+1)} \textbf{ for the calculation of the } n_{sr} \textbf{ rail step: } r_{kn_{sr}}\\
&p_{n_{sr},2}\left\{\begin{pmatrix} w_{h_0}^{n_{sr}-1} & r_{kn_{sr}-1} \\ w_{h_1}^{n_{sr}-1} & r_{kn_{sr}-1} \\ \vdots & \vdots \\ w_{h_{n_{sw}-1}}^{n_{sr}-1} & r_{kn_{sr}-1} \end{pmatrix} \rightarrow \begin{pmatrix} r_{kn_{sr}}^{(1)} \\ r_{kn_{sr}}^{(2)} \\ \vdots \\ r_{kn_{sr}}^{(n_{sw})} \end{pmatrix} \rightarrow r_{kn_{sr}}\right.
\end{aligned}
\tag{65}
$$

where $w_{h_i}^{j}$ indicates, for the hth wheelset, the ith step of the wheel profile that evolves on jth step of the kth rail profile r_{kj} (with $0 \le i \le n_{sw} - 1$, $0 \le j \le n_{sr} - 1$, $1 \le h \le N_w/2$ and $1 \le k \le N_C$). The initial profiles $w_{h_0}^{j}$ are always the same for each j and correspond to the unworn wheel profile (ORE S1002).

Initially the wheel (starting from the unworn profile $w_{h_0}^{0}$) evolves on the unworn rail profile r_{k0} in order to produce the discrete wheel profiles $w_{h_0}^{0}, w_{h_1}^{0}, \ldots, w_{h_{n_{sw}}}^{0}$ (step $p_{1,1}$).

Author's personal copy

Table 10 Computational time

Wear model	Processor	Computational time	
		Dynamic simulation	Wear simulation
UNIFI	INTEL Xeon CPU E 5430 2.66 GHz 8 GB RAM	38 min	9 min
Simpack		1 h 2 min	4 min

Table 11 Integrator parameters

Integrator type	ODE5
Algorithm	Dormand–Prince
Order	5
Step type	Fixed
Step size	10^{-4} s

Then the virtual rail profiles $r_{k1}^{(i+1)}$, obtained by means of the simulations $(w_{h_i}^0, r_{k0})$, are arithmetically averaged so as to get the update rail profile r_{k1} (step $p_{1,2}$). This procedure can be repeated n_{sr} times in order to perform all the rail discrete steps (up to the step $p_{n_{\mathrm{sr}},2}$).

The computational effort required by the simulation strategy is the following:

(a) In the wheel wear study, for each update of the rail profiles r_{kj} (n_{sr} updates), the whole wheel wear loop $w_{h_i}^{\ j}$ (n_{sw} steps of simulation) is simulated. The computational effort results of $n_{\mathrm{sw}} \times n_{\mathrm{sr}} = 75$ steps both for the dynamic analysis and for the wear model necessary to calculate the removed material on the wheel.

(b) In the rail wear study the dynamic analysis are the same as the previous case because for each rail step the wheel profiles $w_{h_i}^{\ j}$ are simulated on r_{kj} in order to obtain $r_k^{\ (i+1)}_j$ and thus the updated rail profiles r_{kj+1} by means of an arithmetic mean. Therefore, no additional dynamical analyses are needed. In this case only the wear model steps ($n_{\mathrm{sw}} \times n_{\mathrm{sr}} = 75$) must be simulated so as to get the removed material on the rail.

The characteristics of the processor used in the simulations and the mean computational times relative to each discrete step of the whole model loop (dynamical simulation and wear simulation including both wheel and rail procedures) are schematically summarized in Table 10 both for the innovative developed model and for the Simpack model. The main numerical parameters relative to the integrator used for the dynamical simulations of both models are briefly reported in Table 11.

The UNIFI dynamic simulation, thanks to the high numerical efficiency of the new global contact model (see Sect. 3.2.1), is rather faster than the Simpack one despite the latter uses approximated look-up tables for evaluating the global contact parameters. In particular the analytical reduction of the algebraic contact problem dimension (from 4D to 1D scalar problem) performed in the UNIFI global contact model implies both an increase of the model efficiency and a simplified treatment of the multiple contact, with a consequent computational time reduction. Moreover the UNIFI innovative algorithm is implemented directly online trough C/C++ user routine strongly integrated within Simpack environment that, consequently, leads to an important improve in terms of computational load and memory consumption (no heavy LUTs are used). On the other hand the approximation due to the global wear evaluation approach of the Simpack model leads to a lower wear simulation time than the UNIFI model where the contact patch investigation obviously has an impact

Author's personal copy

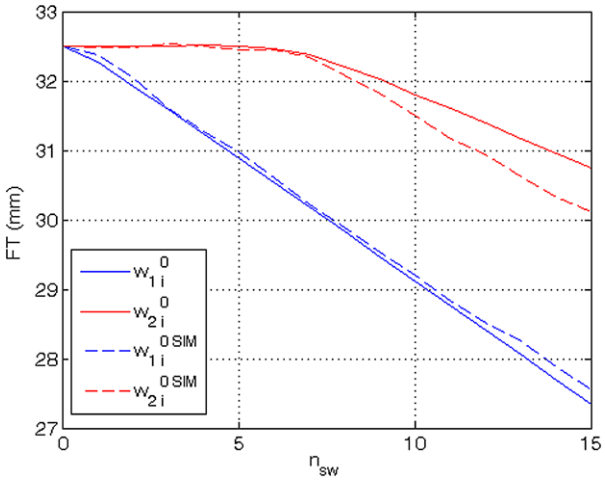

Fig. 18 E.464 vehicle: FT progress at r_{k0} rail step

on the computational load. Finally the UNIFI model highlights a considerable computational time reduction if compared to the Simpack model (almost 30 %).

5.4 Evolution of wear control parameter

In this section the evolution both of the wheel reference quota (flange thickness FT, flange height FH and flange steepness QR) and of the rail reference quota QM numerically evaluated by means of the developed wear model will be compared with the Simpack model results. The wheel quota are shown as a function of the n_{sw} wheel steps while the QM parameter is shown as a function of the rail steps n_{sr}. For reasons of brevity only the wheel quota related to the first and the last rail steps (r_{k0} and r_{k4}) will be shown together with the rail quota QM related to only three of the N_c curves; the considerations on the wheel and rail wear evolution as function of the traveled distance will be presented at the end of this section considering the difference between the discrete step lengths calculated by the two models.

In Figs. 18, 19, 20, and 21 the comparison between the FT dimensions for the two wheelsets of the front bogie of the E.464 locomotive and of the Vivalto coach is presented. As can be seen the thickness of the leading wheel (w_{1i}, ${w_{1i}}^{\mathrm{SIM}}$) decreases more than the same quantity of the rear wheel (w_{2i}, ${w_{2i}}^{\mathrm{SIM}}$) for both vehicles. It is due to the vehicle dynamics (different load distribution on the wheels) and to the particular position of the wheelsets inside the bogie; the rear wheel of each bogie has a smooth curve entry because of the guide effect of the bogie itself.

The FH quota progress is represented in Figs. 22, 23, 24, and 25 and shows that the wheel wear on the tread is appreciable mainly for the first rail step (i.e. UIC60 unworn rail profile), due to the more conformal contact between wheel and rail surface as the rail wear increases. Also the FH dimension displays more wear on the leading wheel while for the rear wheel the tread wear is lower in all studied cases.

The QR trend are shown in Figs. 26, 27, 28, and 29; the flange steepness decreases leading to an increase of the conicity of the flange; also for this dimension the considerations related to the leading and rear wheels hold.

In Fig. 30 the QM evolution for the wear rail can be seen: for the sake of clarity the wear progress of only three of the N_c curves are represented (the first, the 16th and the

Author's personal copy

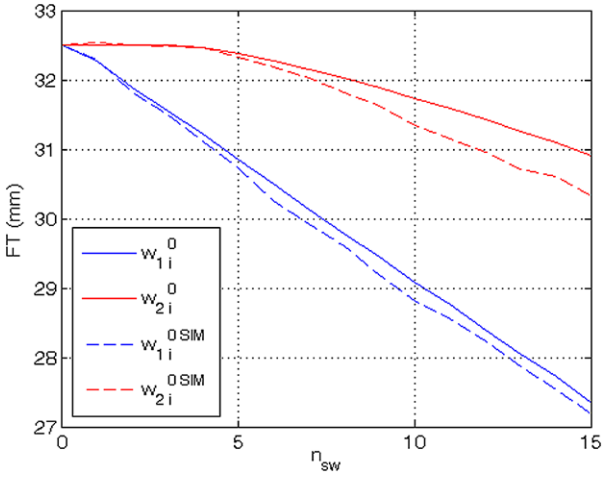

Fig. 19 Vivalto vehicle: FT progress at r_{k0} rail step

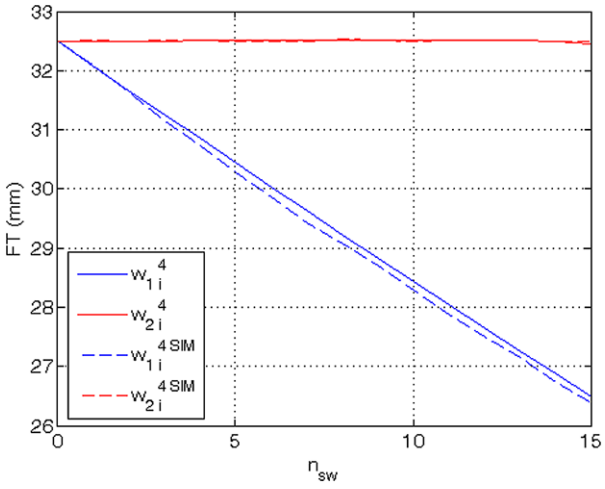

Fig. 20 E.464 vehicle: FT progress at r_{k4} rail step

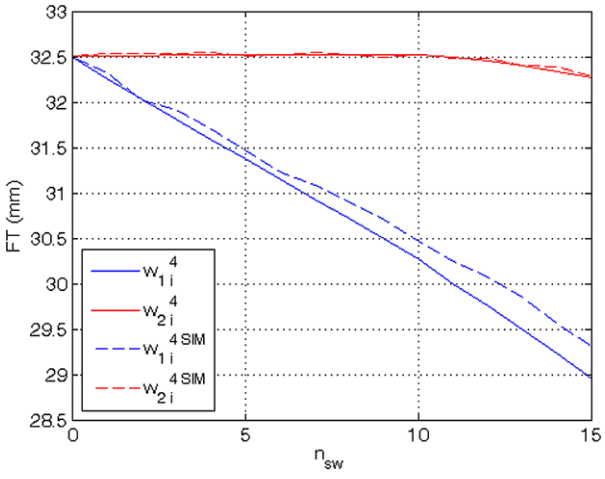

Fig. 21 Vivalto vehicle: FT progress at r_{k4} rail step

Author's personal copy

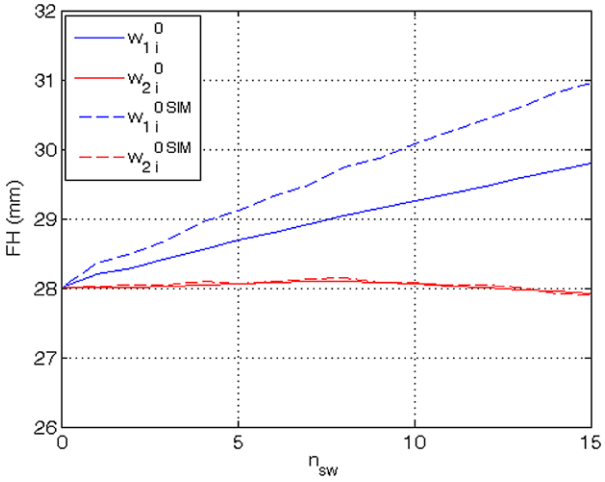

Fig. 22 E.464 vehicle: FH progress at r_{k0} rail step

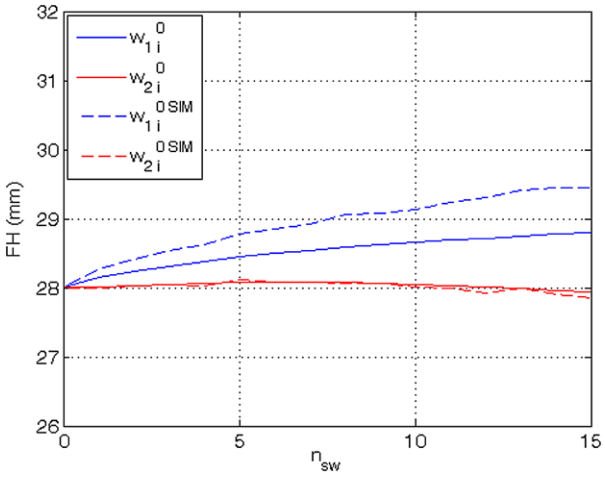

Fig. 23 Vivalto vehicle: FH progress at r_{k0} rail step

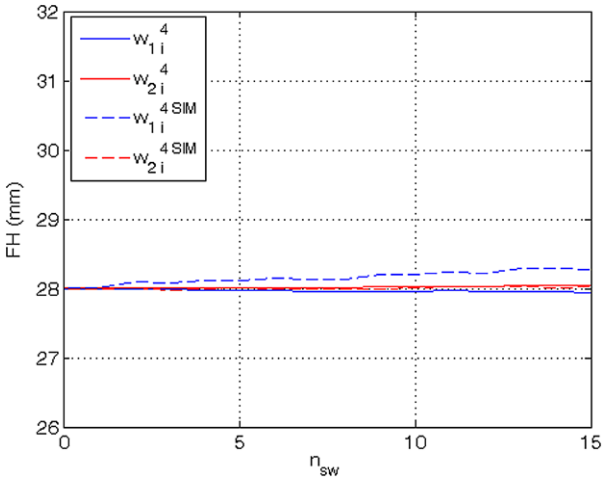

Fig. 24 E.464 vehicle: FH progress at r_{k4} rail step

Author's personal copy

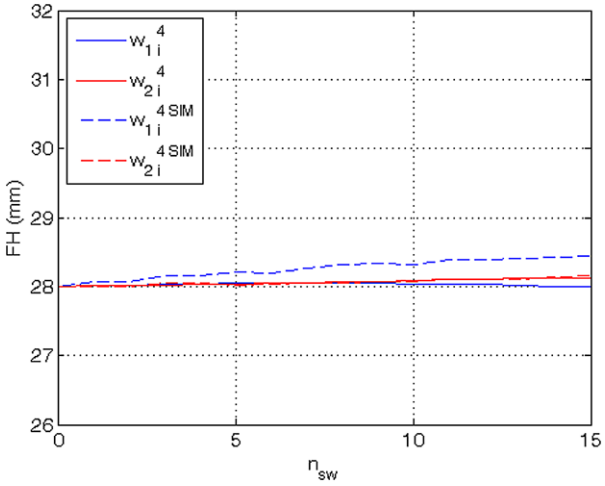

Fig. 25 Vivalto vehicle: FH progress at r_{k4} rail step

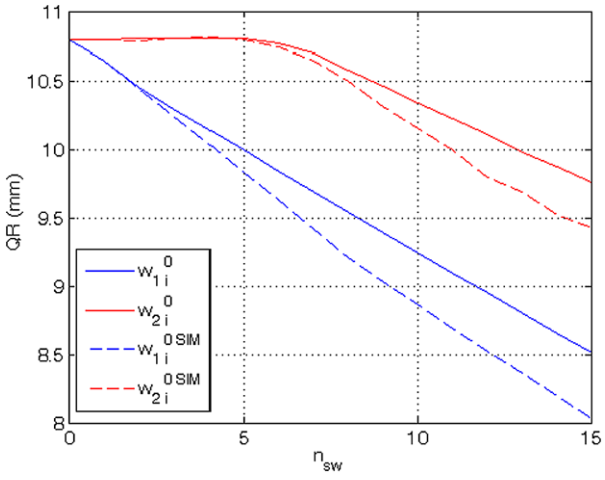

Fig. 26 E.464 vehicle: QR progress at r_{k0} rail step

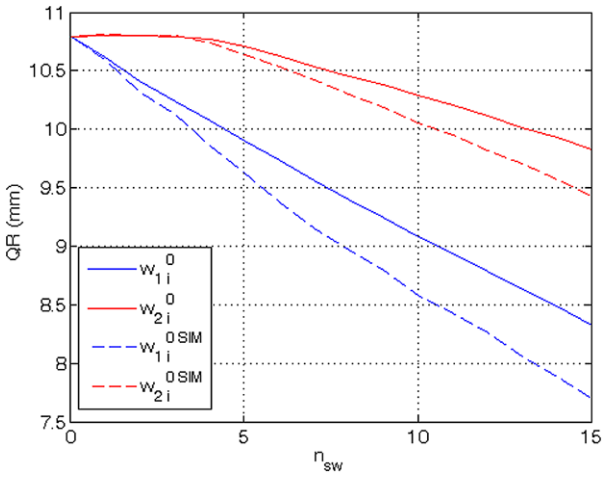

Fig. 27 Vivalto vehicle: QR progress at r_{k0} rail step

Author's personal copy

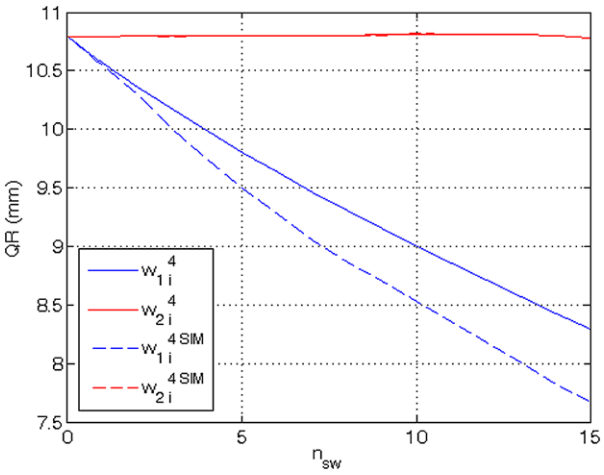

Fig. 28 E.464 vehicle: QR progress at r_{k4} rail step

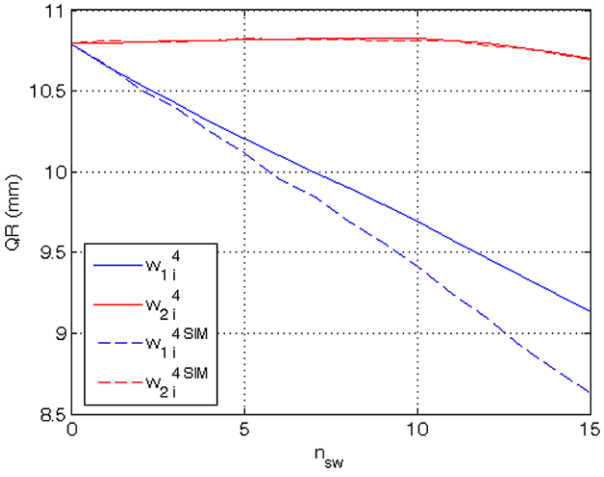

Fig. 29 Vivalto vehicle: QR progress at r_{k4} rail step

31st curves). The QM trend shows that the rail wear increases if the curve radius decreases according with the real wear phenomena (see Table 9: r_{1j} is referred to the minimum curve radius, r_{16j} to an intermediate one while r_{31j} to the maximum curve radius).

In conclusion the comparison of the reference dimensions leads to a good qualitative agreement between the developed wear model and the Simpack one; both show the same wear behavior concerning leading and rear wheelsets, contact conformity and curve radius.

In Fig. 31 the evolution of the $\mathrm{km_{step}}$ as a function of the wheel discrete step number n_{sw} is shown (for brevity only the $\mathrm{km_{step}}$ related to the first and the latter rail step are presented). Related to the first rail step r_{k0}, the lower $\mathrm{km_{step}}$ values and their higher gradient in the first wheel steps indicate the higher wear rate due to the initial non-conformal contact characterizing the coupling between the new ORE S1002 wheel profile and the rail profile UIC60 with laying angle equal to 1/20; the almost constant values in the latter steps (combined with higher $\mathrm{km_{step}}$ values) show at the same time the achievement of a more and more conformal contact as the wheel wear increases. Considering the latter rail step r_{k4} the same curve trend can be seen but characterized by higher $\mathrm{km_{step}}$ values because of the worn rail

Author's personal copy

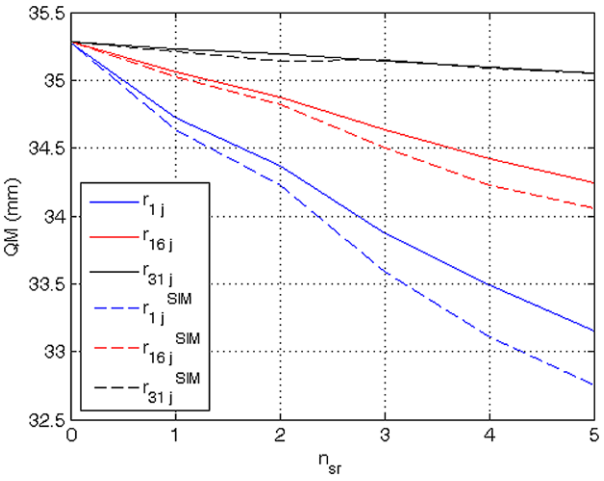

Fig. 30 QM progress

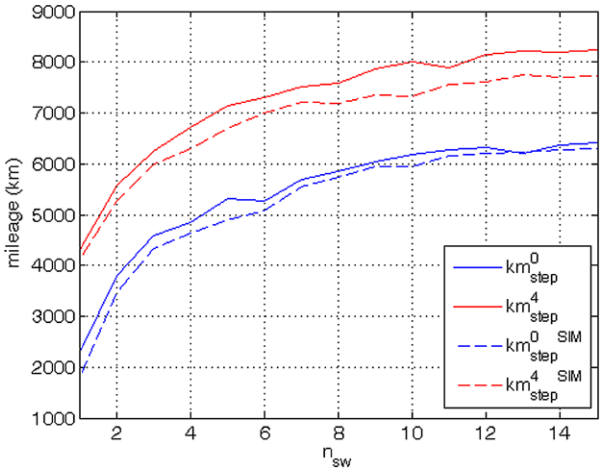

Fig. 31 Evolution of the $\mathrm{km}_{\mathrm{step}}$

Table 12 Evolution of the total mileage $\mathrm{km}_{\mathrm{tot}}$

Wear model	$\mathrm{km}^0_{\mathrm{tot}}$ (km)	$\mathrm{km}^1_{\mathrm{tot}}$ (km)	$\mathrm{km}^2_{\mathrm{tot}}$ (km)	$\mathrm{km}^3_{\mathrm{tot}}$ (km)	$\mathrm{km}^4_{\mathrm{tot}}$ (km)
UNIFI	81460	88120	94350	102080	108950
Simpack	78530	84870	92020	98210	102790

profile that leads to an initial more conformal contact than the previous case. In Fig. 32 the evolution of the N_{step} as a function of the rail discrete number n_{sr} is shown and it can be seen that the considerations referred to the variation of the contact conditions (i.e. non-conformal and conformal contact) hold also in this case.

Tables 12 and 13 show the overall mileages $\mathrm{km}^j_{\mathrm{tot}}$ traveled by the vehicle composition for each rail step $r_{k\,j}$ and the total vehicle number N_{tot} burden on the track during the overall wear loop. The increase of the total mileage as the rail profile is more and more worn is caused by the increase of the conformity between wheel and rail surfaces.

Author's personal copy

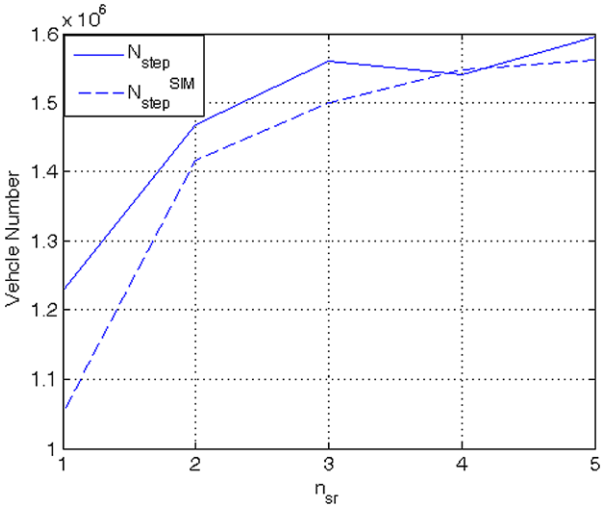

Fig. 32 Evolution of the N_{step}

Table 13 Evolution of the total vehicle number N_{tot}

Wear model	N_{tot}
UNIFI	7390900
Simpack	7074500

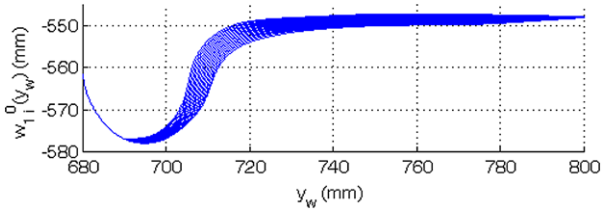

Fig. 33 UNIFI model: E.464 $w_{1_i}^0$ profile evolution

Finally, analyzing the difference between the UNIFI and the Simpack model, Fig. 31 shows slightly lower km_{step} values in the Simpack case that indicate an increase of the wheel wear due to a probable wear overestimation caused by the global wear approach of the Simpack model that, not considering the subdivision of the contact patch in slip and adhesion zone, leads to subtract the mean removed material due to wear in overall the contact patch itself; the same observation holds for the vehicle number N_{step} as can be seen in Fig. 32.

5.5 Evolution of the wheel and rail profile

The wear evolution on the wheel profiles evolving on the first and on the latter rail steps r_{k0}, r_{k4} for the wheelsets of the front bogie of both E.464 and Vivalto vehicles is presented in Figs. 33–48. As stated previously, the wheel profile evolution is described by means of $n_{\text{sw}} = 15$ steps and the threshold on the removed material for each step D_{step}^{w} has been chosen equal to 0.4 mm. From the figures it can be seen both the wear increase on the leading wheel with respect to the rear wheel of the bogie and the wheel wear decrease when the wheel is coupled with the worn rail profile r_{k4} (with respect to the unworn profile r_{k0}) due to the achievement of a more conformal contact in the wheel–rail pairs.

Author's personal copy

Fig. 34 Simpack model: E.464 $w_{1_i}^0$ profile evolution

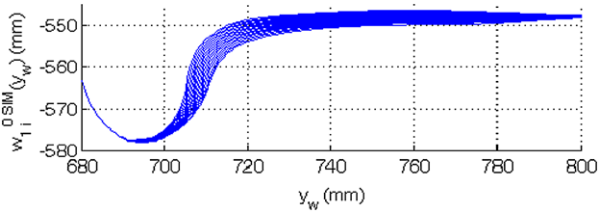

Fig. 35 UNIFI model: E.464 $w_{2_i}^0$ profile evolution

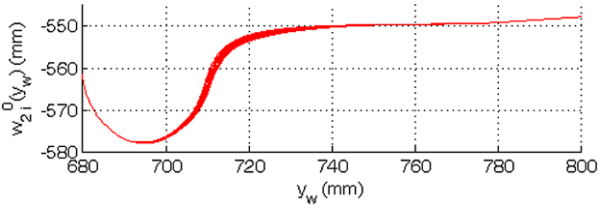

Fig. 36 Simpack model: E.464 $w_{2_i}^0$ profile evolution

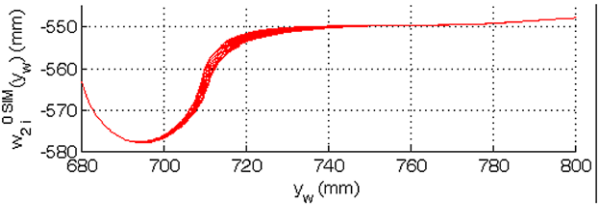

Fig. 37 UNIFI model: Vivalto $w_{1_i}^0$ profile evolution

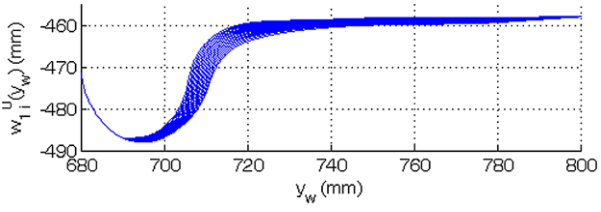

Fig. 38 Simpack model: Vivalto $w_{1_i}^0$ profile evolution

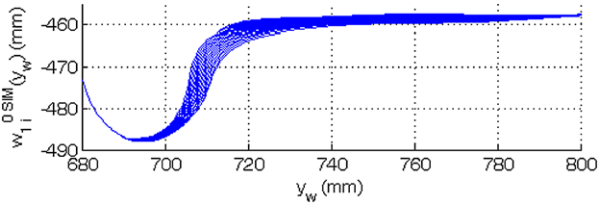

Fig. 39 UNIFI model: Vivalto $w_{2_i}^0$ profile evolution

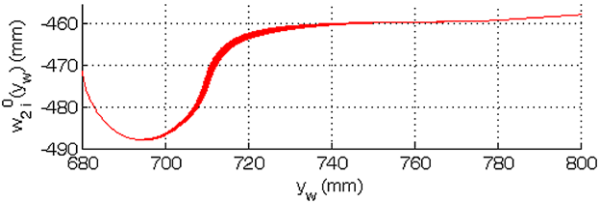

Author's personal copy

Fig. 40 Simpack model: Vivalto $w_{2_i}^0$ profile evolution

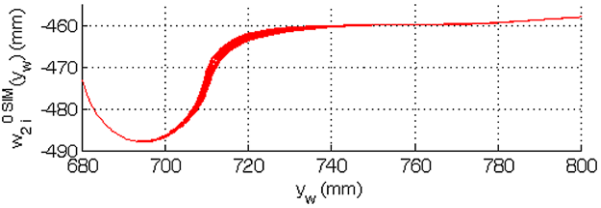

Fig. 41 UNIFI model: E.464 $w_{1_i}^4$ profile evolution

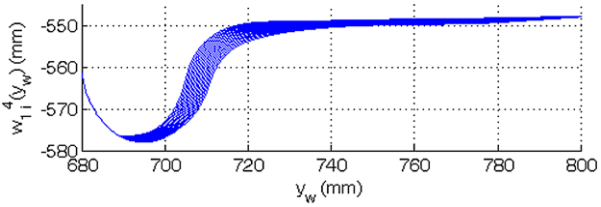

Fig. 42 Simpack model: E.464 $w_{1_i}^4$ profile evolution

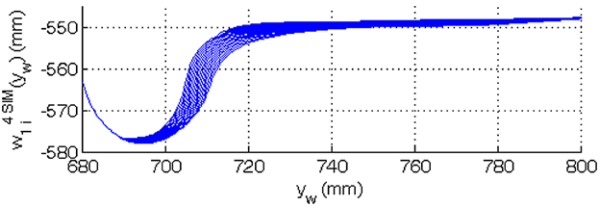

Fig. 43 UNIFI model: E.464 $w_{2_i}^4$ profile evolution

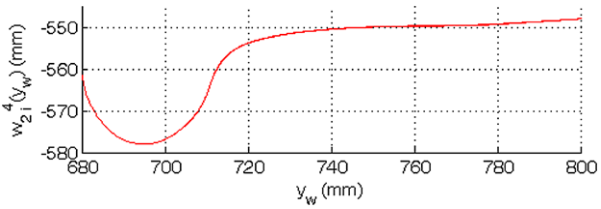

Fig. 44 Simpack model: E.464 $w_{2_i}^4$ profile evolution

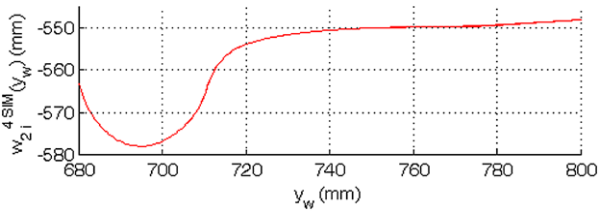

Fig. 45 UNIFI model: Vivalto $w_{1_i}^4$ profile evolution

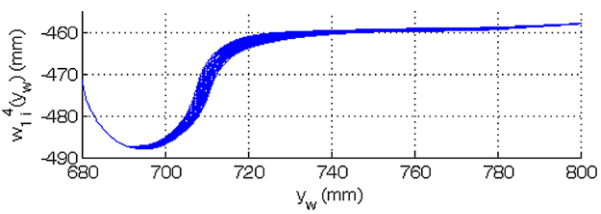

Author's personal copy

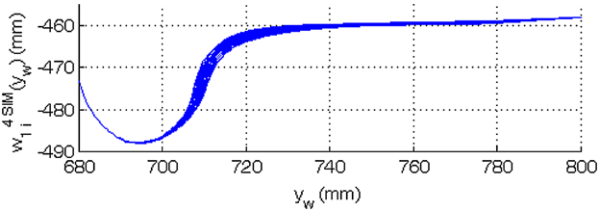

Fig. 46 Simpack model: Vivalto $w_{1_i}^4$ profile evolution

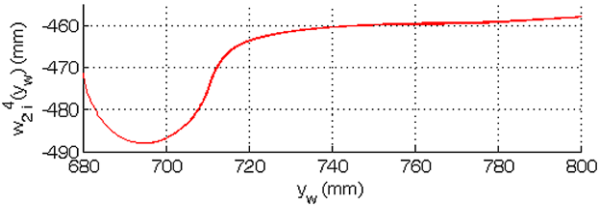

Fig. 47 UNIFI model: Vivalto $w_{2_i}^4$ profile evolution

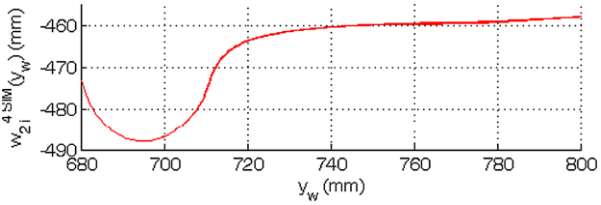

Fig. 48 Simpack model: Vivalto $w_{2_i}^4$ profile evolution

By way of example, Figs. 49 and 50 show the cumulative distributions of removed material in vertical direction z_w on the leading wheel profile of the E.464 locomotive at the first and at the last rail step $\sigma_{w1_{\mathrm{Kw}}}{}^{0}(y_w) = \sum_{i=1}^{\mathrm{Kw}} \sigma_i^{w1\,0}(y_w)$ and $\sigma_{w1_{\mathrm{Kw}}}{}^{n_{\mathrm{sr}}-1}(y_w) = \sum_{i=1}^{\mathrm{Kw}} \sigma_i^{w1\,n_{\mathrm{sr}}-1}(y_w)$ as a function of y_w $(1 \leq \mathrm{Kw} \leq n_{\mathrm{sw}})$; $\sigma_i^{w1\,j}(y_w)$ is the removed material between two subsequent discrete steps of the leading wheel profile evolution (the ith and the $(i-1)$th wheel discrete steps) at the jth rail step $(0 \leq j \leq n_{\mathrm{sr}} - 1)$ (for reasons of clarity only the distributions characterized by $\mathrm{Kw} = 1, 8, n_{\mathrm{sw}}$ are represented). The cumulative distributions highlight the reduction of removed material as the contact becomes more and more conformal.

In Figs. 51–56 the rail profile evolutions related to the three different curves of the statistical analysis $r_{1\,j}$, $r_{16\,j}$ and $r_{31\,j}$ are presented; the removed material due to wear shows a rather clear dependence from the curve radius and in particular the wear increases in the sharp curves because of the resulting vehicle dynamics and harder contact conditions. For instance, Fig. 57 shows the cumulative distributions of removed material on the rail (in vertical direction z_r) of the first curve of the statistical analysis $\sigma_{r1_{\mathrm{Kr}}}(y_r) = \sum_{j=1}^{\mathrm{Kr}} \sigma_j^{r1}(y_r)$ as a function of y_r $(1 \leq \mathrm{Kr} \leq n_{\mathrm{sr}})$; $\sigma_j^{r1}(y_r)$ is the removed material between two subsequent discrete steps of the rail profile evolution (the jth and the $(j-1)$th rail discrete steps).

In all the studied cases the comparison between the profile evolution obtained with the innovative developed wear model and the Simpack one results rather satisfactory without pronounced differences.

Author's personal copy

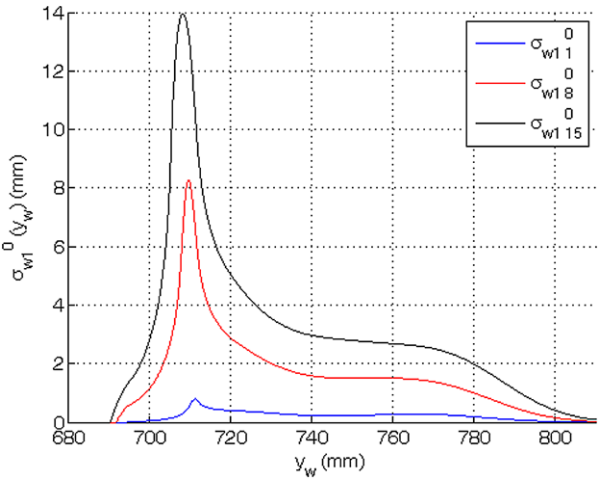

Fig. 49 UNIFI model: E.464 cumulative distributions $\sigma_{w1_i}^{0}$ of the removed wheel material

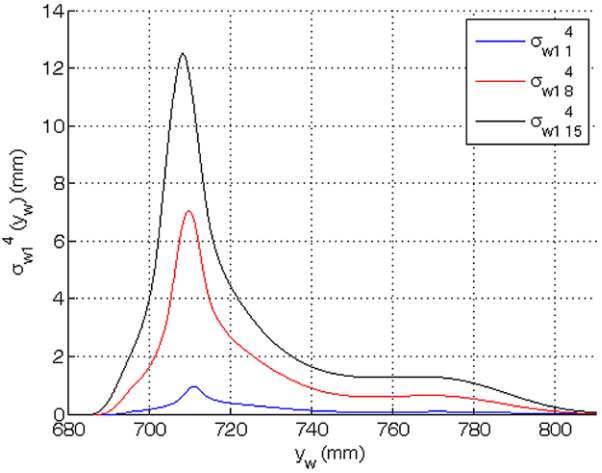

Fig. 50 UNIFI model: E.464 cumulative distributions $\sigma_{w1_i}^{4}$ of the removed wheel material

6 Conclusions

In this work the Authors presented a complete model for the wheel and rail wear prediction in railway application, developed thanks to the collaboration with Trenitalia S.p.A and Rete Ferroviaria Italiana (RFI), which provided the necessary technical data referred to a vehicle composition widely used in Italian railways (E.464 locomotiveand Vivalto coach) and to the track data related to the whole Italian railway network. The whole model is made up of two mutually interactive parts. The first one evaluates the vehicle dynamics and comprises both the multibody model of the vehicle implemented in Simpack and a global wheel–rail contact model (developed by the authors in previous works) for the calculation of the contact points and of the contact forces. The second one is the wear model (composed by the local contact model, the wear evaluation procedure and the profile update strategy) which, starting from

Author's personal copy

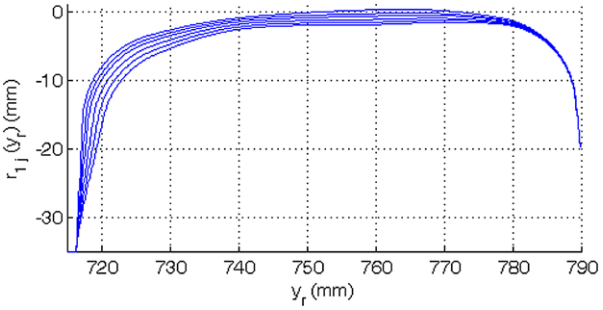

Fig. 51 UNIFI model: $r_{1\,j}$ profile evolution

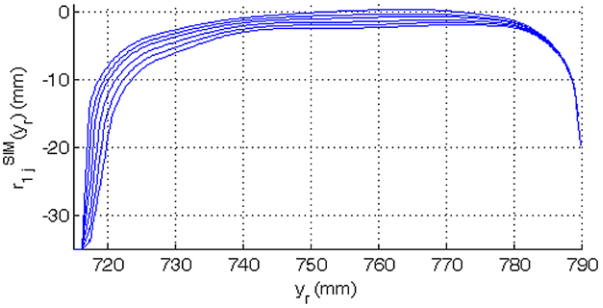

Fig. 52 Simpack model: $r_{1\,j}{}^{\mathrm{SIM}}$ profile evolution

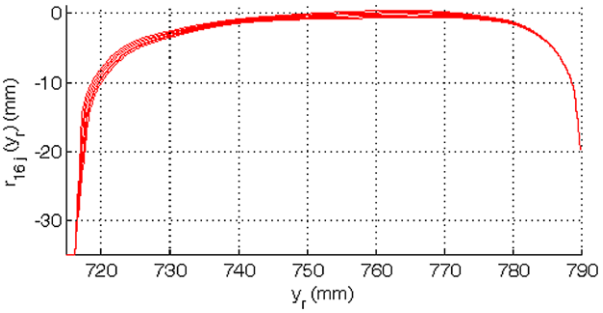

Fig. 53 UNIFI model: $r_{16\,j}$ profile evolution

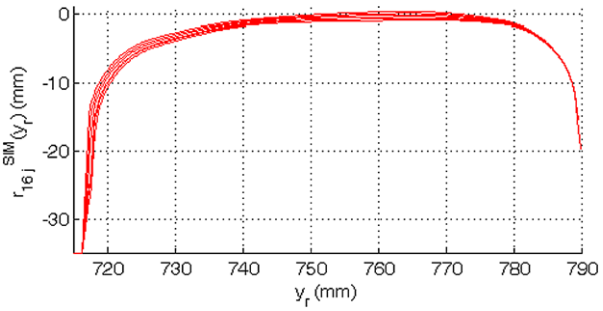

Fig. 54 Simpack model: $r_{16\,j}{}^{\mathrm{SIM}}$ profile evolution

Author's personal copy

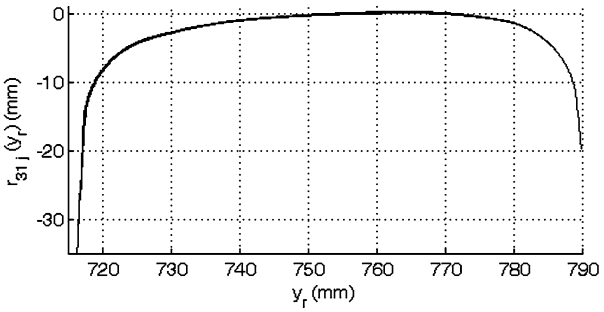

Fig. 55 UNIFI model: $r_{31\,j}$ profile evolution

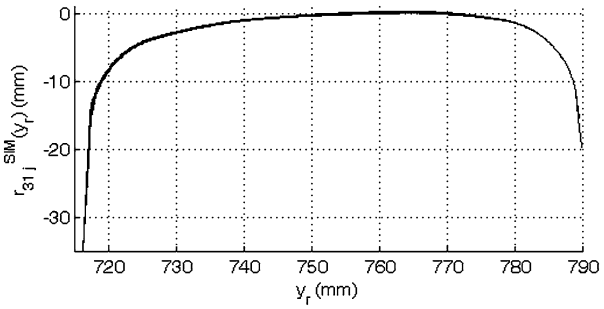

Fig. 56 Simpack model: $r_{31\,j}^{\mathrm{SIM}}$ profile evolution

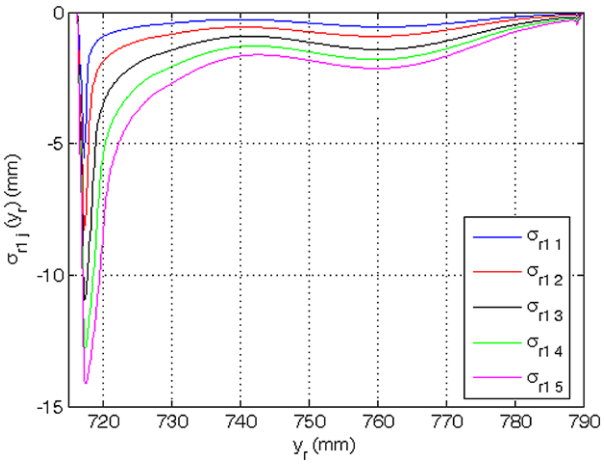

Fig. 57 UNIFI model: cumulative distributions $\sigma_{r1\,j}$ of the removed rail material

the outputs of the multibody simulations, evaluates the amount of material to be removed due to wear. The interaction between the two parts is not a continuous time process but occurs at discrete steps; consequently the evolution of the wheel and rail geometry is described through several intermediate profiles.

In particular a suitable profile update algorithm has been developed in order to consider the different time scales characterizing the wheel and rail wear evolutions: the wheel wear has been studied basing on the distance traveled by vehicle, while the rail wear has been evaluated basing on the total tonnage burden on the railway track.

Author's personal copy

The performance of the innovative model have been compared with the wear evaluation procedure implemented within the Simpack multibody commercial software in order to have a further validation of the model besides the wheel wear validation referred to the quite short critical scenario of the Aosta–Pre Saint Didier line performed in previous works [6, 7]. The comparison has been carried out, from the track viewpoint, on the whole Italian railway network modeled through an innovative statistical approach; in particular the network has been described by means of a set of simpler tracks statistically equivalent to the original line on which the simulations have been performed.

The results obtained in this research highlight how the innovative model reflects the real behavior of the wear phenomena (for example a higher removed material for the leading wheel and for the sharp curves and a wear decrease when the contact conditions reach the conformal contact). The comparison with the Simpack wear model has given satisfactory results both in terms of reference dimensions and profiles evolution; the only difference is a little wear overestimation of the Simpack model probably due to the approximated global wear approach that does not consider the division of the contact patch in adhesion and slip zone. Moreover the innovative model highlights better performance in terms of computational efficiency with a considerable time reduction if compared to the Simpack model (almost 30 %).

Future developments will be based on further experimental data (relative to other railway tracks with a higher mileage than the Aosta–Pre Saint Didier line used in previous works) provided by Trenitalia and RFI and referred to advanced wear on the wheel (especially on the wheel tread) and on the rail. In this way other analysis will be carried out in order to further validate the whole model. Subsequently the design of new wheel and rail profiles as well as of new bogie shapes and suspension stages optimized from the wear viewpoint will be performed according to the research interests of Trenitalia. Finally, a code optimization, concerning the vehicle model (in particular the global contact model), the wear model, and the whole loop (interaction between Matlab and Simpack environment) is scheduled for the future in order to reduce the simulation times.

Acknowledgements Authors would like to thank Engg. R. Cheli and G. Grande of Trenitalia S.p.A. for providing and giving the permission to edit the data relative to the vehicle composed by the E.464 locomotive and the Vivalto passenger coach; a special thanks also goes to the Engg. R. Mele and M. Finocchi of Rete Ferroviaria Italiana for the data relative to the whole Italian railway network.

References

1. Krause, H., Poll, G.: Verschleißbei gleitender und wälzender Relativbewegung. Tribol. Schmier.tech. **31**(4/5), 209–214/285–289 (1984)
2. Specht, W.: Beitrag zur rechnerischen Bestimmung des Rad- und Schienenverschleisses durch Gueterwagen Diss. RWTH Aachen (1985)
3. Pombo, J., Ambrosio, J., Pereira, M., Lewis, R., Dwyer-Joyce, R., Ariaudo, C., Kuka, N.: A study on wear evaluation of railway wheels based on multibody dynamics and wear computation. Multibody Syst. Dyn. **24**, 347–366 (2010)
4. Jendel, T., Berg, M.: Prediction of wheel profile wear. Suppl. Veh. Syst. Dyn. **37**, 502–513 (2002)
5. Zobory, I.: Prediction of wheel/rail profile wear. Veh. Syst. Dyn. **28**, 221–259 (1997)
6. Ignesti, M., Malvezzi, M., Marini, L., Meli, E., Rindi, A.: Development of a wear model for the prediction of wheel and rail profile evolution in railway systems. Wear **284–285**, 1–17 (2012)
7. Auciello, J., Ignesti, M., Malvezzi, M., Meli, E., Rindi, A.: Development and validation of a wear model for the analysis of the wheel profile evolution in railway vehicles. Veh. Syst. Dyn. **50**(11), 1707–1734 (2012)
8. Braghin, F., Lewis, R., Dwyer-Joyce, R.S., Bruni, S.: A mathematical model to predict railway wheel profile evolution due to wear. Wear **261**, 1253–1264 (2006)

Author's personal copy

9. Hardwick, C., Lewis, R., Eadie, D.: Wheel and rail wear—understanding the effect of third body materials. In: CM2012 9th International Conference on Contact Mechanics and Wear of Rail/Wheel Systems, Chengdu, China (2012)
10. Meli, E., Falomi, S., Malvezzi, M., Rindi, A.: Determination of wheel–rail contact points with semianalytic methods. Multibody Syst. Dyn. **271**, 238–245 (2008)
11. Auciello, J., Meli, E., Falomi, S., Malvezzi, M.: Dynamic simulation of railway vehicles: wheel/rail contact analysis. Veh. Syst. Dyn. **47**, 867–899 (2009)
12. Hertz, H.: The contact of elastic solids. J. Reine Angew. Math. **92**, 156–171 (1881)
13. Kalker, J.J.: Three-Dimensional Elastic Bodies in Rolling Contact. Kluwer Academic, Dordrecht (1990)
14. Kalker, J.J.: Survey of wheel–rail rolling contact theory. Veh. Syst. Dyn. **8**, 317–358 (1979)
15. Enblom, R., Berg, M.: Simulation of railway wheel profile development due to wear influence of disc braking and contact environment. Wear **258**, 1055–1063 (2005)
16. Official site of Simpack GmbH (2012). http://www.simpack.com
17. Pombo, J., Ambrosio, J., Pereira, M., Lewis, R., Dwyer-Joyce, R., Ariaudo, C., Kuka, N.: Development of a wear prediction tool for steel railway wheels using three alternative wear functions. Wear **20**, 327–358 (2011)
18. Toni, P.: Ottimizzazione dei profili delle ruote su binario con posa 1/20. Tech. rep., Trenitalia S.p.A. (2010)
19. Iwnicki, S.: The Manchester Benchmarks for Rail Vehicle Simulators. Swets and Zeitlinger, Lisse (1999)
20. Meli, E., Magheri, S., Malvezzi, M., Rindi, A.: An innovative wheel–rail contact model for multibody applications. Wear **271**, 462–471 (2011)
21. Meli, E., Magheri, S., Malvezzi, M.: Development and implementation of a differential elastic wheel–rail contact model for multibody applications. Veh. Syst. Dyn. **49**(6), 969–1001 (2011)
22. Johnson, K.: Contact Mechanics. Cambridge University Press, Cambridge (1985)
23. Shabana, A.A., Tobaa, M., Sugiyama, H., Zaazaa, K.E.: On the computer formulations of the wheel/rail contact problem. Nonlinear Dyn. **40**, 169–193 (2005)
24. Iwnicki, S.: Simulation of wheel–rail contact forces. Fatigue Fract. Eng. Mater. Struct. **26**, 887–900 (2003)
25. Kalker, J.J.: A fast algorithm for the simplified theory of rolling contact. Veh. Syst. Dyn. **11**, 1–13 (1982)
26. EN 14363: Railway applications—Testing for the acceptance of running characteristics of railway vehicles—Testing of running behavior and stationary tests (2005)
27. EN 15313: Railway applications—In-service wheelset operation requirements—In-service and off-vehicle wheelset maintenance (2010)
28. Oppenheim, A., Schafer, R.W.: Discrete-Time Signal Processing. Prentice-Hall, Englewood Cliffs (1989)
29. Esveld, C.: Modern railway track. Delft University of Technology, Delft, Netherlands, 2001 (1985)